Mathematical Model of an Adult Human Atrial Cell
The Role of K^+ Currents in Repolarization

A. Nygren, C. Fiset, L. Firek, J.W. Clark, D.S. Lindblad, R.B. Clark, W.R. Giles

Abstract—We have developed a mathematical model of the human atrial myocyte based on averaged voltage-clamp data recorded from isolated single myocytes. Our model consists of a Hodgkin-Huxley–type equivalent circuit for the sarcolemma, coupled with a fluid compartment model, which accounts for changes in ionic concentrations in the cytoplasm as well as in the sarcoplasmic reticulum. This formulation can reconstruct action potential data that are representative of recordings from a majority of human atrial cells in our laboratory and therefore provides a biophysically based account of the underlying ionic currents. This work is based in part on a previous model of the rabbit atrial myocyte published by our group and was motivated by differences in some of the repolarizing currents between human and rabbit atrium. We have therefore given particular attention to the sustained outward K^+ current (I_{sus}), which putatively has a prominent role in determining the duration of the human atrial action potential. Our results demonstrate that the action potential shape during the peak and plateau phases is determined primarily by transient outward K^+ current, I_{sus}, and L-type Ca^{2+} current ($I_{Ca,L}$) and that the role of I_{sus} in the human atrial action potential can be modulated by the baseline sizes of $I_{Ca,L}$, I_{sus}, and the rapid delayed rectifier K^+ current. As a result, our simulations suggest that the functional role of I_{sus} can depend on the physiological/disease state of the cell. **(*Circ Res*. 1998;82:63-81.)**

Key Words: human atrium ■ repolarization ■ sustained outward current ■ computer modeling ■ cardiac action potential

Within the past 5 years, quite extensive voltage-clamp and action potential data from human atrial myocytes have been published from a number of laboratories. In most cases the human atrial tissue was obtained during open heart surgery, in which small pieces of the right atrial appendage are excised as part of the cannulation procedure for cardiopulmonary bypass. However, cardiac tissue can also be obtained from the free wall of the atrium during valve replacement procedures, from explanted failing hearts during heart transplantations, or from donor hearts that cannot be used for transplantation. Once a specimen of cardiac tissue is obtained, enzymatic dispersion techniques are used to isolate single cardiac cells, from which action potential and voltage-clamp data can be recorded. We have made recordings of the outward K^+ currents, which are responsible for repolarization in human atrial myocytes.[1,2] On the basis of these data, as well as other published results, we have developed the first comprehensive mathematical model of the electrophysiological responses of a representative human atrial cell.

There are a number of published mathematical models that simulate the electrophysiological responses in several different species and cardiac cell types. Examples include the Purkinje fiber model of DiFrancesco and Noble,[3] the Hilgemann and Noble atrial model,[4] the Earm and Noble model of the single atrial cell,[5] the bullfrog atrial and sinus venosus models of Rasmusson and colleagues,[6,7] the ventricular cell models of Luo and Rudy,[8–11] the rabbit sinoatrial node cell model of Demir et al,[12] and the rabbit atrial cell model of Lindblad et al.[13] Recently, the emphasis has shifted from general models, based on voltage-clamp data from several species,[3,4] to more detailed models based on data from single isolated cells from a particular species. This is a direct reflection of the progress made in experimental work and the resulting availability of more comprehensive data. Our goal was to develop a model that is sufficiently accurate to have predictive capabilities for selected aspects of the electrophysiological responses in human atrium. Emphasis has been placed on the functional roles of the K^+ currents during repolarization.

Materials and Methods

Basic Assumptions

Our model is of the general type first introduced by DiFrancesco and Noble[3] and is based, in part, on the rabbit atrial model of Lindblad, Murphey, Clark, and Giles[13] (hereafter referred to as the LMCG model). As shown in Fig 1, the model consists of a Hodgkin-Huxley–type electrical equivalent circuit for the sarcolemma coupled with a fluid compartment model. The dimensions of the human atrial myocyte are assumed identical to those of the rabbit atrial cell in the LMCG model. These dimensions (cylindrical geometry of 130-μm length and 11-μm diameter) are very close to the dimensions of human atrial myocytes (eg, 120-μm length and 10- to 15-μm diameter[14]). In addition, we have used a total cell capacitance of 50 pF,which agrees very well with our experimental observations for human atrial myocytes (51.9±3.5 pF, n=52).

Received June 9, 1997; accepted September 30, 1997.

From the Department of Electrical and Computer Engineering (A.N., J.W.C., D.S.L.), Rice University, Houston, Tex, and the Department of Physiology and Biophysics (C.F., L.F., R.B.C., W.R.G.), University of Calgary (Canada) Medical School.

Correspondence to Dr J.W. Clark, Department of Electrical and Computer Engineering, Rice University, 6100 South Main, Houston, TX 77005-1892. E-mail jwc@rice.edu

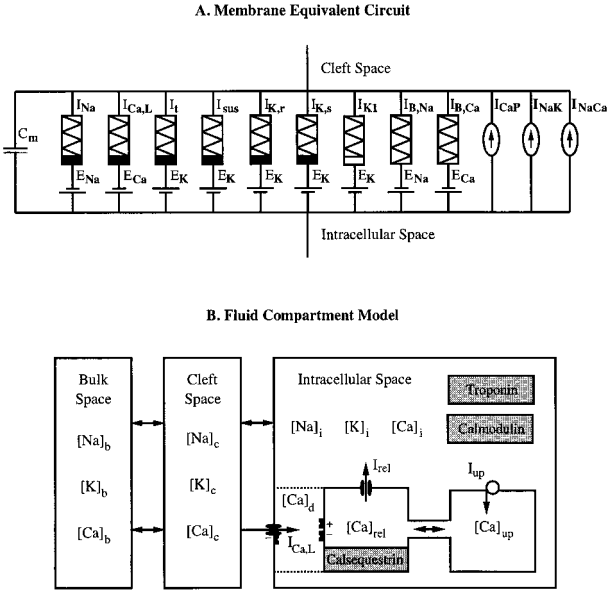

Figure 1. Schematic representation of the mathematical model of the human atrial cell. A, Electrical equivalent circuit for the sarcolemma. B, Fluid compartment model, including intracellular, cleft, and extracellular spaces.

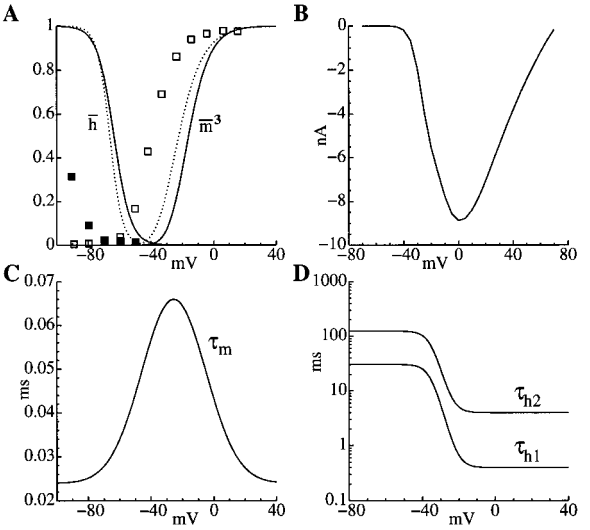

Figure 2. Parameters for I_{Na}. A, Steady-state activation ($\bar{m}^3$) and inactivation ($\bar{h}$) (□ and ■ represent data from Sakakibara et al[15] and dotted lines the expressions used in the LMCG model[13]). B, Simulated peak current-voltage relationship. C, Activation time constant (τ_m). D, Inactivation time constants (τ_{h1} and τ_{h2}).

Membrane Currents

Fig 1A shows the electrical equivalent circuit for the sarcolemma of the human atrial cell. It includes each of the ionic currents that are known to contribute to the action potential in human atrial myocytes (I_{Na}, $I_{Ca,L}$, I_t, I_{sus}, $I_{K,r}$, $I_{K,s}$, and I_{K1}), the Ca^{2+} and Na^+-K^+ pump and Na^+-Ca^{2+} exchanger currents responsible for maintaining intracellular ion concentrations (I_{CaP}, I_{NaK}, and I_{NaCa}), and the Na^+ and Ca^{2+} background (leakage) currents ($I_{B,Na}$ and $I_{B,Ca}$). Mathematical expressions describing the time and voltage dependence of the ionic currents have been developed on the basis of published voltage-clamp data recorded predominantly from human atrial myocytes. (See "Glossary" after Appendix 2 for terms used in text, figures, and tables.)

Na^+ Current: I_{Na}

Voltage-clamp data for I_{Na} in human atrial and ventricular myocytes, recorded at 17°C have been published by Sakakibara and colleagues.[15,16] These data suggest that the activation threshold is very close to the resting potential (≈−75 mV), which seems unrealistic, given that atrial and ventricular cells exhibit stable resting potentials and thresholds for activation near −55 mV. Moreover, the steady-state inactivation curves measured by Sakakibara and colleagues[15,16] are such that I_{Na} would be completely inactivated (ie, no current available) at the resting potential. As pointed out by these authors, this is probably a result of time- and/or temperature-dependent shifts in the steady-state inactivation characteristics. Other results, such as the data from rabbit atrium published by Wendt et al[17] (on which the I_{Na} description in the LMCG model is based) yield more positive (depolarized) steady-state activation and inactivation curves.

In developing a model of I_{Na} under physiological conditions, we have found it necessary to use indirect information about I_{Na} provided by action potential data in addition to voltage-clamp data. Thus, we have adjusted the steady-state activation curve ($\bar{m}^3$) for I_{Na} so that the threshold at which an action potential is elicited agrees with experimental observations. Furthermore, the peak magnitude of I_{Na} was adjusted to match the maximum upstroke velocity of the action potential. (For a discussion of the relation between I_{Na} and action potential upstroke velocity, refer to Cohen and Strichartz.[18]) Fig 2A shows the steady-state activation ($\bar{m}^3$) and inactivation ($\bar{h}$) curves used to model I_{Na}. Compared with the data from human atrial myocytes obtained by Sakakibara et al[15] (Fig 2A), there are significant positive shifts in both the $\bar{m}^3$ (+22.8 mV) and the $\bar{h}$ (+32.2 mV) curves. Fig 2B shows a simulated peak current-voltage relationship (steps from a holding potential of −80 mV) for I_{Na}. The mathematical expressions for the kinetics of activation (τ_m) and inactivation (τ_{h1} and τ_{h2}) are very similar to those of the LMCG model, as shown in Figs 2C and 2D. The processes of inactivation and recovery from inactivation are both described by the sum of a fast and a slow exponential. At plateau potentials, the fast component of inactivation has a time constant of 0.3 ms. The slow component of inactivation accounts for 10% of the total current and has a time constant of 3.0 ms at plateau potentials; ie, it is 10 times slower than the fast component, in agreement with the data of Sakakibara et al.[15]

L-Type Ca^{2+} Current: $I_{Ca,L}$

Several quite comprehensive studies of $I_{Ca,L}$ in human atrial myocytes have been published.[19–25] Overall, the results are quite consistent: $I_{Ca,L}$ has an activation threshold near −40 mV, its peak at ≈0 mV, and an apparent reversal potential of +50 to +60 mV. The current density for $I_{Ca,L}$ varies considerably among these studies, however, and is also known to be reduced in diseased or dilated cells.[22,26] Table 1 shows published $I_{Ca,L}$ densities compared with those used in the present model. The inactivation process for $I_{Ca,L}$ is usually described as the sum of a fast and a slow component.[19–23] In order to accurately measure the steady-state voltage dependence of inactivation, the duration of the "conditioning" prepulse in the voltage-clamp protocol (eg, see Li and Nattel[25]) must be at least four to five times the time constant of the slower component of inactivation. If the prepulse duration is shorter, the slower component will not have reached its steady state when the availability of current is measured (second voltage-clamp pulse), and inactivation will appear incomplete. Ouadid et al[24] measured inactivation at room temperature (where the slower time constant exceeds

TABLE 1. Peak $I_{Ca,L}$ Values From the Literature Compared With the Model

	Peak $I_{Ca,L}$		
Reference	**Normal**	**Diseased/Dilated**	**Temperature**
Li and Nattel[25]	−11 pA/pF	...	36°C
Mewes and Ravens[23]	−1.5 pA/pF	...	21°C to 23°C
Ouadid et al[26]	−12 pA/pF	−2 pA/pF	22°C
Le Grand et al[22]	−17 pA/pF	−5 pA/pF	20°C to 24°C
Model	−4.5 pA/pF	...	33°C

100 ms[23]) and found that inactivation was incomplete (U-shaped inactivation curve) when the prepulse duration was 150 ms but that it became more complete if the prepulse duration was increased to 400 ms. The data obtained by Li and Nattel at 36°C yield almost complete inactivation characteristics for a prepulse duration of 150 ms, consistent with faster kinetics at this temperature. However, these authors also note that prolonging the prepulse results in more complete inactivation curves. On the basis of these results, we have modeled inactivation of $I_{Ca,L}$ as a process involving two components with different time constants but identical, fully inactivating, steady-state voltage dependence. This formulation differs from the LMCG model[13] as well as the Luo-Rudy model,[9] which both use a single (voltage-dependent) component of inactivation with incomplete steady-state voltage dependence.

Ouadid et al[24] also report that the inactivation process is slowed considerably when Ba^{2+} is substituted for Ca^{2+} as charge carrier, indicating that inactivation is also Ca^{2+} dependent. This phenomenon is included in the Luo-Rudy model[9] but not in the LMCG model.[13] Our formulation differs from that of Luo and Rudy, however, in order to incorporate recent experimental results. First, there is now evidence that there exists a small restricted subsarcolemmal domain between the L-type Ca^{2+} channels and the peripheral junctional sarcoplasmic reticulum (SR) where Ca^{2+} concentration ($[Ca^{2+}]_d$) may transiently reach much higher levels than in the cytosol as a whole.[27] This subsarcolemmal domain is not included in the Luo-Rudy model, which models Ca^{2+}-dependent inactivation as a function of total cytosolic Ca^{2+} concentration. We have included such a subsarcolemmal domain and have modeled Ca^{2+}-dependent inactivation as a function of $[Ca^{2+}]_d$. Second, there is recent evidence to suggest that $[Ca^{2+}]_d$ modulates $I_{Ca,L}$ inactivation by promoting a rapid mode of inactivation.[28,29] Therefore, in our model, $[Ca^{2+}]_d$ determines the fraction of L-type channels that are in the rapidly inactivating mode, ie, the ratio of the fast to slow components of inactivation discussed above. Thus, in this model, an experiment with Ba^{2+} as charge carrier shifted this equilibrium so that all L-type channels were in the slow mode. With Ca^{2+} as charge carrier, however, the equilibrium is shifted toward the faster mode of inactivation by an amount determined by $[Ca^{2+}]_d$. Hence, the inactivation of the total $I_{Ca,L}$ follows a biexponential time course, where the relative contributions of the fast and slow exponentials are determined by $[Ca^{2+}]_d$. We have chosen to model this $[Ca^{2+}]_d$ dependence as an instantaneous function of $[Ca^{2+}]_d$, assuming that the shift between the two modes is rapid compared with the diffusion of Ca^{2+} out of the restricted domain.

Fig 3A shows the steady-state activation (d_L) and inactivation (f_L) curves used to model $I_{Ca,L}$. Assuming that activation can be measured more accurately at room temperature than at physiological temperature, we have used the activation curve (d_L) measured by Mewes and Ravens.[23] However, in order to fit the voltage-clamp data (peak currents) of Li and Nattel[25] (Fig 3B), we found it necessary to shift this activation curve by +3 mV. The expression for the inactivation curve (f_L) is identical to that reported by Li and Nattel for human atrial myocytes at physiological temperature. Furthermore, the reversal potential for $I_{Ca,L}$ is set to a constant value of +60.0 mV, as measured by Li and Nattel, rather than to the Nernst potential for Ca^{2+} ions. As shown in Fig 3B, the simulated peak current-voltage relationship (steps from a holding potential of −80 mV) agrees well with voltage-clamp data. Figs 3C and 3D show the time constants of activation (τ_{dL}) and inactivation (τ_{fL1} and τ_{fL2}) plotted against membrane voltage. We have used the inactivation and recovery time constant data obtained by Li and Nattel to formulate the expressions for τ_{fL1} and τ_{fL2} (see Fig 3D). These data were obtained in human atrial myocytes at physiological temperature. The expression for τ_{dL} (Fig 3C) is similar to that of the LMCG model.

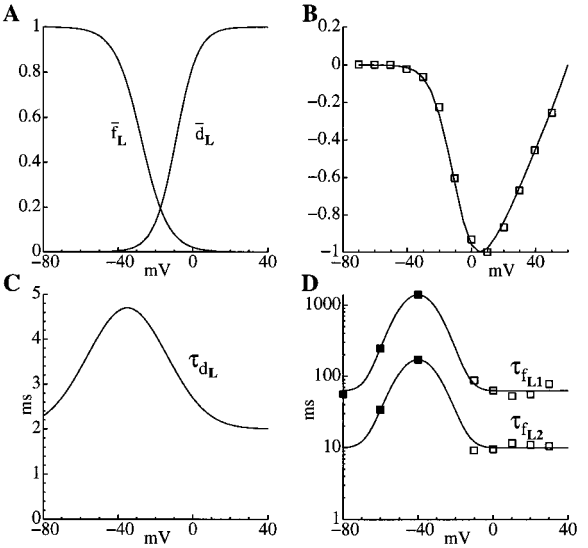

Figure 3. Parameters for $I_{Ca,L}$. A, Steady-state activation ($\bar{d}_L$) and inactivation ($\bar{f}_L$) curves. B, Simulated peak current-voltage relationship, normalized to peak current (□ represents data from Li and Nattel[25]). C, Activation time constant (τ_{dL}). D, Inactivation time constants (τ_{fL1} and τ_{fL2}), with data from Li et al[25] (■, recovery; □, inactivation).

Transient and Sustained Outward K^+ Currents: I_t and I_{sus}

Voltage-clamp experiments designed to study the outward currents responsible for repolarization in human atrial myocytes have identified a transient outward K^+ current (denoted I_t), which activates rapidly on depolarization.[1,30] In addition to this (Ca^{2+}-independent) transient K^+ current, a Ca^{2+}-dependent transient outward current, which is activated by relatively large increases in $[Ca^{2+}]_i$, is sometimes observed.[31] We have chosen not to include this Ca^{2+}-dependent current, since it has never been observed in our experimental work. After I_t has decayed (inactivated), a more slowly inactivating, "sustained," outward K^+ current (denoted I_{sus}) is observed.[2,22,32,33] The available data suggest that I_{sus} is a separate current from I_t and that it is also carried mainly by K^+ ions.[2,34,35]

The literature regarding the voltage dependence of I_t is somewhat inconsistent. In particular, the results regarding steady-state activation vary considerably. Shibata et al[1] report a half-activation voltage ($V_{1/2}$) of +1.0 mV for I_t in human atrium, whereas Näbauer et al,[36] Wettwer et al[33] (both in studies of human ventricle), and Le Grand et al[22] (human atrium) report values of +16.7, +20.6, and +33.3 mV, respectively. These results seem unrealistic, since I_t is known to have a strong influence on early repolarization,[1,2] and these values of $V_{1/2}$ would result in only a small amount of I_t current being activated during a normal action potential (peak at +20 to +30 mV). Among the possible explanations for this variability in $V_{1/2}$ are the sensitivity of this parameter to the concentration of divalent cations (Cd^{2+} and Co^{2+}) used to block $I_{Ca,L}$[33,37] and the possibility of a difference between human atrial and ventricular I_t. Therefore, we have based our model on the data of Shibata et al,[1] which were recorded from human atrium in the presence of a low (100 μmol/L) $[Cd^{2+}]$. The data regarding the voltage dependence of steady-state inactivation are also variable between different studies. Fig 4A shows the steady-state activation ($\bar{r}$) and inactivation ($\bar{s}$) curves used to model I_t. The $\bar{r}$ curve is based on a fit to data from Shibata et al (○ in Fig 4A), and the $\bar{s}$ curve is that reported by Firek and Giles.[2] Time constants of activation (τ_r) and inactivation (τ_s) are plotted against voltage in Fig 4C and 4D, respectively. Data regarding the time constant of inactivation[2] indicate that τ_s is ≈13 ms (at 33°C) at membrane voltages positive to 0 mV. At hyperpolarized potentials, the recovery of I_t from inactivation as measured in our laboratory appears to follow an exponential time course with a strongly voltage-dependent time constant, increasing from 15 ms at −100 mV to 387 ms at −60 mV. Our formulation for τ_s is based on a fit to experimentally obtained recovery time constant values at negative potentials and inactivation time constant values at positive potentials. The recovery of I_t from inactivation in human atrial cells has been shown to be considerably more rapid than in rabbit atrial cells.[2,38] As a result, I_t magnitude and action potential waveshape are much less rate dependent in human atrial cells.

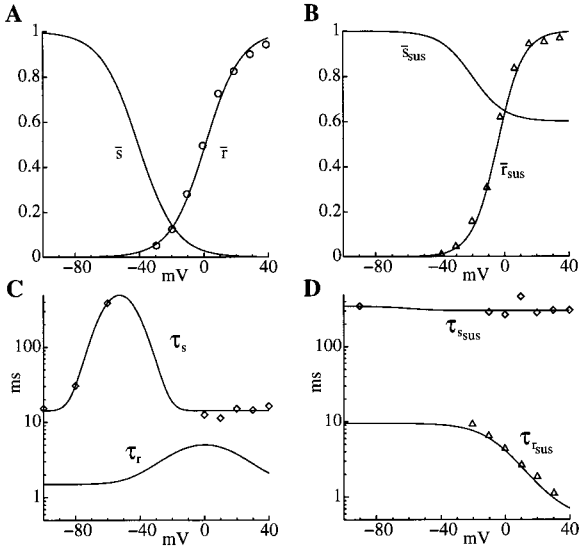

Figure 4. Parameters for I_t and I_{sus}. A, Steady-state activation and inactivation curves for I_t ($\bar{r}$ and $\bar{s}$, respectively) (○ represents data from Shibata et al[1]). B, Steady-state activation and inactivation curves for I_{sus} ($\bar{r}_{sus}$ and $\bar{s}_{sus}$, respectively) (△ represents data from Wang et al[35]). C, Activation and inactivation time constants for I_t (τ_r and τ_s, respectively). D, Activation and inactivation time constants for I_{sus} (τ_{rsus} and τ_{ssus}, respectively) (△ represents data from Wang et al[35]).

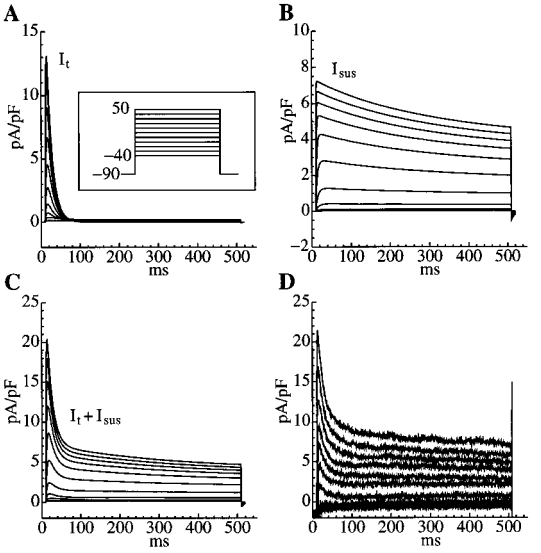

Figure 5. I_t and I_{sus} in response to the voltage-clamp protocol shown in the inset, normalized to cell capacitance. A, Simulated I_t waveforms. B, Simulated I_{sus} waveforms. C, Sum of the I_t and I_{sus} waveforms in panels A and B. D, Outward currents recorded from a human atrial myocyte.

Our model of I_{sus} is based on the data of Wang et al.[35] Fig 4B and 4D show the steady-state activation curve (r_{sus}) and time constant of activation (τ_{rsus}) for this current. On the basis of our recent data, we have also included a slow ($\tau \approx 300.0$ ms) partial (40%) inactivation. The time constant for this inactivation process was obtained by fitting a biexponential function to the decaying outward current waveforms as described by Koidl et al.[39] In addition to providing an estimate of τ_{ssus}, this method also provides a more accurate separation of I_t and I_{sus} than when I_{sus} is estimated as the current at the end of the pulse.[2,35,40] By combining our models of I_t and I_{sus}, we are able to produce current waveforms closely resembling those recorded from human atrial myocytes in response to voltage-clamp pulses. Fig 5 shows how I_t (panel A) and I_{sus} (panel B) combine (panel C) to produce waveforms similar to experimental results (panel D). In our experience, the size of these currents varies considerably between individual cells, and as reported by Amos et al,[40] there is also considerable variability in the ratio of I_t to I_{sus}. The sizes of I_t and I_{sus} in the model were chosen to provide good fits to action potential data and are well within this experimental variability. Table 2 compares I_t and I_{sus} densities reported in the literature with those used in this model.

Delayed Rectifier K^+ Currents: $I_{K,r}$ and $I_{K,s}$

Recent studies of the delayed rectifier K^+ currents in human and rabbit atrial myocytes show that in both species the delayed rectifier current is generated by two distinct K^+ conductances. These "rapid" ($I_{K,r}$) and "slow" ($I_{K,s}$) conductances have significantly different properties and can be separated experimentally on the basis of, for example, the sensitivity of $I_{K,r}$, but not $I_{K,s}$, to the antiarrhythmic drug E-4031.[41–43] Since $I_{K,s}$ is believed to contribute only a small fraction of the total delayed rectifier current during a normal atrial action potential,[41] one could produce an acceptable fit to nominal action potential data using a model incorporating only $I_{K,r}$. However, because of the very slow activation characteristics of $I_{K,s}$, this current would be expected to be more significant at high heart rates, where it could build up progressively from cycle to cycle as a result of residual activation, ie, failure to decay completely between cycles. Therefore, we have chosen to include both $I_{K,r}$ and $I_{K,s}$ in our model, thus enabling it to simulate specific effects of antiarrhythmic drugs on $I_{K,r}$, the buildup of $I_{K,s}$ at elevated heart rates, and the resulting changes, such as those in action potential duration (APD) and refractory period.

Our model of $I_{K,r}$ is based on data from Wang et al,[44] Muraki et al,[41] and Sanguinetti et al.[45] Figs 6A and 6C show the steady-state activation ($\bar{p}_a$) and inactivation ($\bar{p}_i$) curves and the time constant of activation (τ_{pa}) compared with the available data. Since the inactivation of $I_{K,r}$ is very rapid compared with the activation, inactivation is modeled as being instantaneous. The expressions for $I_{K,s}$ are based on data recorded in human atrial myocytes by Wang and colleagues.[42,44] Figs 6B and 6D show the characteristics of this current.

In order to verify our model of $I_{K,r}$ we chose to simulate the "ramp clamp" experiment of Muraki et al[41] in rabbit atrial cells (their Fig 7), in which the cell is subjected to an 0.8-V/s repolarizing ramp from an action potential peak potential down to −80 mV. This waveform is an approximation to the repolarization phase of an atrial action potential. The result (simulated response) is shown in Fig 7, along with data from Muraki et al. Note that the simulated waveform is very similar, although in order to fit action potential data, we have had to reduce the size of $I_{K,r}$ to 15% of that shown in Fig 7. Given that it is often difficult to detect any delayed rectifier current at all in most human atrial myocytes,[2] it seems reasonable that this current should be assigned a very low density.

Time-Independent Currents: I_{K1}, $I_{B,Na}$, $I_{B,Ca}$, I_{NaK}, I_{NaCa}, and I_{CaP}

In the absence of reliable published data from human atrial cells for these currents, we have used expressions from the LMCG model[13] with only minor scaling adjustments. One exception is the inward

TABLE 2. Values for I_t and I_{sus} at +40 mV From the Literature Compared With the Model

Reference	I_t	I_{sus}	Temperature
Koidl et al[39]*	8 pA/pF	13 pA/pF	36°C to 37°C
Amos et al[40]†	5 pA/pF	6 pA/pF	22°C
Wang et al[35]†	...	4 pA/pF‡	25°C
Our data*	13.4 pA/pF	6.0 pA/pF	33°C
Model	11.1 pA/pF	6.7 pA/pF	33°C

*I_t and I_{sus} separated by curve-fitting.
†$I_t = I_{peak} - I_{late}$; $I_{sus} = I_{late}$.
‡Mean I_{sus} (≈300 pA) divided by mean capacitance (74.3 pF).

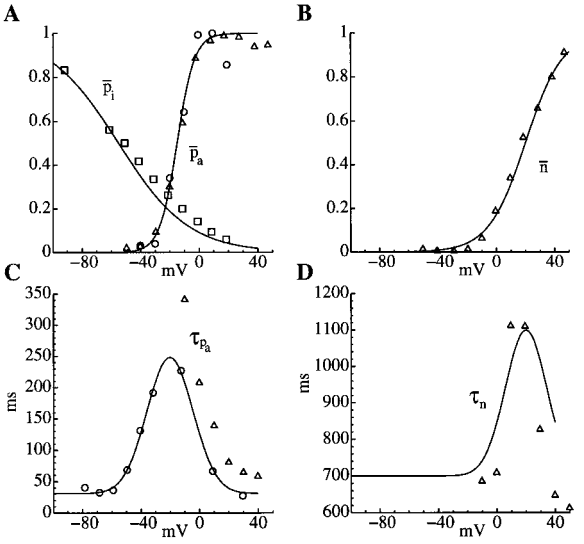

Figure 6. Parameters for $I_{K,r}$ and $I_{K,s}$. A, Steady-state activation and inactivation curves for $I_{K,r}$ ($\bar{p}_a$ and $\bar{p}_i$, respectively). Data are from Wang et al[44] (△), Muraki et al[41] (○), and Sanguinetti et al[45] (□). B, Steady-state activation curve for $I_{K,s}$ ($\bar{n}$). Data are from Wang et al[44] (△). C, Activation time constant for $I_{K,r}$ (τ_{pa}). Data are from Wang et al[44] (△) and Muraki et al[41] (○). D, Activation time constant for $I_{K,s}$ (τ_n). Data are from Wang et al[44] (△).

rectifier current, where we have found it necessary to make minor modifications to the rectifying characteristics in order to fit action potential data (slightly narrower outward "hump"). We have also adjusted the $[K^+]_c$ dependence of I_{K1} to agree with data from our laboratory. Table 3 lists the changes made in the time-independent currents compared with those in the LMCG model.

Material Balance

As in the LMCG model,[13] we have included a fluid compartment formulation to monitor and account for changes in ion concentrations. These concentration changes can be a result of current flow across the cell membrane or of redistribution of ions within the cell (eg, uptake of Ca^{2+} by the SR or binding of Ca^{2+} to an intracellular buffer). Our fluid compartment model is similar to the one in the LMCG model. It includes descriptions of extracellular and intracellular spaces, formulations for Ca^{2+} uptake and release and the buffering action of calsequestrin, and troponin and calmodulin buffers in the intracellular medium. Compartment volumes and other ultrastructural properties, as well as expressions describing the binding of Ca^{2+} to intracellular troponin and calmodulin buffers and to calsequestrin in the SR release

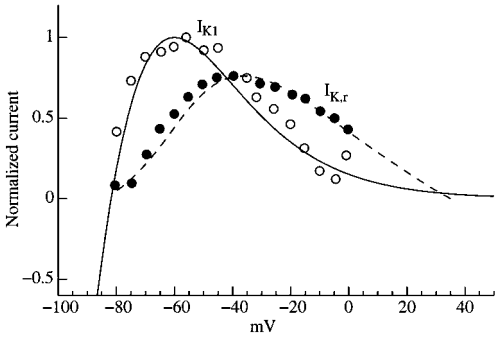

Figure 7. Current-voltage relationship for I_{K1} and $I_{K,r}$ normalized to peak I_{K1} (≈0.6 pA/pF) (○ and ● represent data from Muraki et al[41]). The $I_{K,r}$ waveform is the response to an 0.8-V/s "ramp" repolarization from an action potential peak potential down to −80 mV.[41]

TABLE 3. Time-Independent Current Formulations Compared With the LMCG Model

Current	Changes From LMCG Formulation
I_{K1}	Slightly narrower outward "hump"
	$[K^+]_c$ dependence based on human data
$I_{B,Na}$	5% reduction in $\bar{g}_{B,Na}$
$I_{B,Ca}$	154% increase in $\bar{g}_{B,Ca}$
I_{NaK}	10% increase in $\bar{I}_{NaK}$
I_{NaCa}	87% increase in k_{NaCa}
I_{CaP}	58% reduction in $\bar{I}_{CaP}$

LMCG indicates the model of Lindblad et al.[13]

compartment, are identical to those of the LMCG model, except as noted in the following sections.

Cleft Space

We have included a "cleft space" in our fluid compartment formulation, ie, a small restricted space surrounding the cell, in which accumulation or depletion of ions may occur (see Demir et al[12]). The cleft space is modeled as an unstirred fluid layer; ie, ions can be exchanged between the cleft space and the extracellular medium (in which all concentrations are assumed constant) only through diffusion as a result of a concentration gradient. Ratios between diffusion time constants for the ions involved (τ_{Na}, τ_K, and τ_{Ca}) were calculated from values for ionic conductivity[46] and the composition of the extracellular solution ($[Cl^-]_o$=140 mmol/L, $[Na^+]_o$=130 mmol/L, $[K^+]_o$=5.4 mmol/L, and $[Ca^{2+}]_o$=1.8 mmol/L). We have adjusted the size and diffusion properties of the cleft space so as to produce oscillations in cleft space $[K^+]$ ($[K^+]_c$) similar to experimental data.[47,48]

Electroneutral Na^+ Influx

In order to achieve long-term stability in the ionic concentrations in the model, we have found it necessary to add a small (1.68-pA) electroneutral inward flux of Na^+, denoted $\Phi_{Na,en}$. This flux could, for example, be accounted for in terms of electroneutral coupled transport mechanisms, such as Na^+-H^+ exchange and Na^+-K^+-2Cl cotransport. Modeling of these mechanisms, however, is beyond the scope of this work.

There are two major reasons for including this flux: First, the fact that long-term ionic homeostasis can be achieved with the addition of this small flux demonstrates that the sizes and other characteristics of the model elements are such that ionic homeostasis can reasonably be maintained. Second, if the ionic concentrations were allowed to change slowly from cycle to cycle (which would be the result if this flux were not included), the model would only be valid for short simulation times (seconds), for which this drift can safely be ignored. By ensuring long-term stability of the ionic concentrations, longer simulation times (minutes) become feasible and meaningful. Only with stable ionic concentrations can the model be used to simulate concentration changes as a result of rate changes or other interventions.

Sarcoplasmic Reticulum

Our formulation for the SR is very similar to that of the LMCG model. However, we have made one important modification in accordance with recent evidence demonstrating that Ca^{2+} can accumulate in a small domain between the sarcolemma and the peripheral junctional SR and trigger Ca^{2+} release.[27,49] Specifically, we have removed the voltage-dependent term in the formulation for activation of SR Ca^{2+} release and replaced it with a term dependent on Ca^{2+} concentration in the restricted subsarcolemmal domain, $[Ca^{2+}]_d$. The sole mechanism for SR Ca^{2+} release in our model is therefore Ca^{2+}-induced Ca^{2+} release (CICR). Fig 1B includes a schematic representation of the model of the SR.

Stern[50] has shown that in order for a CICR model to be stable, ie, capable of producing a response that is graded by the amount of Ca^{2+}

that enters the cell through $I_{Ca,L}$, the trigger Ca^{2+} has to be separated from that released from the SR. Anatomically, this can be understood in terms of the concept of "release units" discussed, for example, by Isenberg and Han.[51] According to this concept, Ca^{2+} release from the SR is recruited stepwise by the all-or-none activation of individual release units, consisting of one or more L-type Ca^{2+} channel and associated SR release channels. The activation of a release unit results in CICR within that unit only. The released Ca^{2+} then diffuses into the myoplasm, without directly affecting other units. This phenomenon has been incorporated in our model as a lumped mechanism, where the SR release channel senses $[Ca^{2+}]$ in the restricted domain ($[Ca^{2+}]_d$) but releases Ca^{2+} directly to the cytosol (Fig 1B), thus separating trigger Ca^{2+} from that released from the SR.

Parameter Values

A model of this type contains a large number of parameters that must be assigned values based on the available data. We have approached this part of the model development process in a two-step fashion, where the majority of the parameter values have been assigned in the first step, based on experimental studies of individual model components. This has the advantage that most of the parameters associated with an individual membrane current can be justified and assigned independently. Once the descriptions of individual membrane currents has been completed, one is left with a limited number of free parameters, most of which are scaling factors, such as the maximum conductance values for each ionic current. These remaining free parameters can then be determined using data for whole-cell responses (eg, action potential waveforms) or other constraints as indicated previously (eg, ionic homeostasis). It should be emphasized, however, that model development is very much an iterative process and that it has been necessary in some cases to modify individual current expressions to obtain acceptable fits to action potential data or (as in the case of I_{Na}) to use information from action potential recordings to resolve ambiguities in ion channel current data. The following sections describe the constraints and criteria used in order to assign values for the remaining free parameters.

The Quiescent Human Atrial Myocyte

In the absence of an external stimulus, a healthy human atrial cell is quiescent (does not contract or produce an action potential). In this quiescent state, the membrane potential comes to an equilibrium, "resting," potential at which the net ion flux across the sarcolemma is zero. The resting membrane potential varies somewhat among individual cells, ranging from −70 to −80 mV. The resting membrane potential is the result of a precise balance between the time-independent background, pump, and exchanger currents (I_{K1}, $I_{B,Na}$, $I_{B,Ca}$, I_{NaK}, I_{CaP}, and I_{NaCa}). Although the resting state of the cell may seem less interesting than the active state during an action potential, an accurate description of the resting conditions is, in our experience, essential for successful modeling of the action potential. Moreover, the model of the resting state of the cell determines very important threshold characteristics and subthreshold properties, such as the input resistance of the cell. Very accurate simulation of these passive characteristics is essential before the cell model is to be used in distributed simulations, eg, of the propagation of electrical activity from one cell to another. We have modeled the resting state of the cell by adjusting the magnitudes of these currents so as to produce zero net transmembrane current at a resting potential of ≈75 mV and the following intracellular ion concentrations: $[Na^+]_i \approx 8.5$ mmol/L; $[K^+]_i \approx 130.0$ mmol/L, and $[Ca^{2+}]_i \approx 60.0$ nmol/L. The input resistance of the cell in this quiescent state is ≈600 MΩ, which agrees with our experimentally observed values.

The Activated Human Atrial Myocyte

When the cell is stimulated, it produces an action potential, the shape of which depends on the relative sizes of the ionic currents involved. Action potential data recorded from isolated human atrial myocytes are (in our experience) quite variable from cell to cell. It is therefore questionable whether it is possible to define the "normal human atrial action potential" in a meaningful way. We have chosen to fit our model to an action potential waveform that is representative of what is most often recorded from isolated human atrial cells in our laboratory. By establishing this "nominal model," we have obtained a starting point from which the sensitivity of the action potential waveform to parameter perturbations may be studied (see "Results"). In addition to dictating the action potential waveform, the sizes (maximum conductance parameters) of the ionic currents also affect ionic homeostasis. The membrane currents involved in shaping the action potential therefore have to act in concert with those involved in the resting state to maintain constant ion concentrations at nominal stimulation rates. We have "tuned" our model so that ion concentrations remain constant from cycle to cycle at a stimulus frequency of 1 Hz.

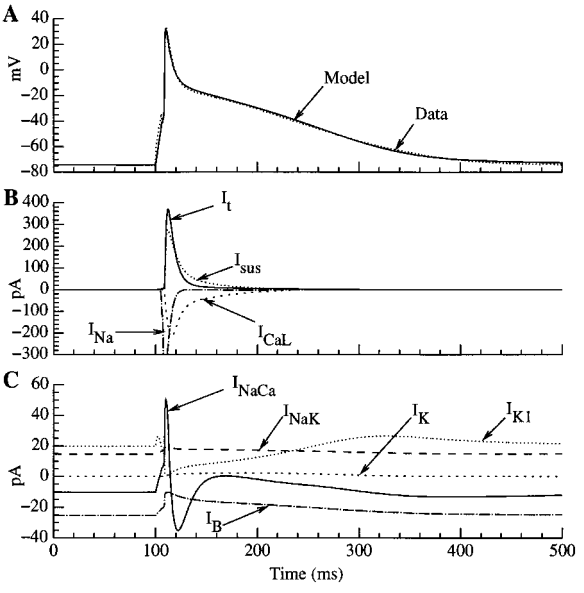

Figure 8. Model-generated action potential and membrane current waveforms. A, Model-generated action potential (solid line) compared with recorded data (dotted line). B and C, Model-generated waveforms for the ionic currents during the action potential (note the difference in scale between panels B and C).

Results

There are two major aims of the simulations presented in the following sections: (1) to establish the validity and usefulness of our model by demonstrating that the expressions that are based on fits to voltage-clamp data for individual ionic currents also are able to accurately reconstruct action potential data and (2) to use the model to investigate the functional roles of different ionic currents, to study the sensitivity of the action potential waveform to the sizes of those currents, and, finally, to predict the whole-cell response to, for example, selected channel blocking drugs.

Simulated Action Potential Waveform

Fig 8A shows a simulated action potential waveform (solid line) compared with an action potential (dotted line) recorded at a temperature of 33°C and a stimulus frequency of 0.5 Hz. There is close agreement between the waveforms (the discrepancy at the beginning of the upstroke is due to a stimulation artifact that is not simulated). As mentioned previously, the action potential waveform varies significantly among individual cells and in multicellular preparations from the human atrium, presumably because of variations in the magnitudes of the underlying ionic currents. Nevertheless, the ability of this model to accurately reproduce a recorded action potential, in

TABLE 4. Current Integrals Over 1 s at Quiescence and at Stimulus Rates of 1 and 2 Hz

	Quiescent			1 Hz			2 Hz		
	Na^+	K^+	Ca^{2+}	Na^+	K^+	Ca^{2+}	Na^+	K^+	Ca^{2+}
Q_{Na}	0.00	...	...	−6.09	...	...	−10.33	...	...
$Q_{B,Na}$	−9.09	...	...	−8.23	...	...	−7.52	...	...
Q_t	...	0.06	...	...	4.80	...	...	7.92	...
Q_{sus}	...	0.00	...	...	5.53	...	...	10.85	...
Q_{K1}	...	19.76	...	...	19.70	...	...	20.84	...
$Q_{K,s}$	...	0.01	...	...	0.19	...	...	0.47	...
$Q_{K,f}$	...	0.00	...	...	0.26	...	...	0.48	...
$Q_{Ca,L}$	...	...	−0.01	...	...	−5.75	...	...	−11.80
$Q_{B,Ca}$	...	...	−16.99	...	...	−15.31	...	...	−13.91
Q_{NaK}	41.01	−27.34	...	45.71	−30.47	...	49.61	−33.07	...
Q_{CaP}	...	...	0.84	...	...	1.26	...	...	1.65
Q_{NaCa}	−24.77	...	16.51	−29.71	...	19.80	−35.53	...	23.68
$Q_{Na,en}$	−1.68	...	...	−1.68	...	...	−1.68	...	...
Q_{tot}	5.46	−7.50	0.36	0.00	0.00	0.00	−5.44	7.49	−0.36

For quiescent and 2-Hz rates, the integrals were computed 20 s after leaving the nominal 1-Hz rate. All values are pC/s.

combination with the previously demonstrated fits to voltage-clamp data, lends credibility to the model.

In Fig 8, panels B and C show the behavior of the membrane currents during an action potential. The first current to respond to a depolarizing stimulus pulse (delivered at time=100 ms) is I_{Na}, which activates rapidly, resulting in a very large but transient inward current. Note that I_{Na} is too large to be shown on the scale of Fig 8B; its peak magnitude is ≈−5.8 nA, which corresponds to a maximum upstroke velocity of 116 V/s. I_{Na} is primarily responsible for the upstroke (phase 0) of the action potential, but as seen from Fig 8B, a substantial amount of I_{Na} remains during the early peak phase of the action potential as a result of the second slower component of I_{Na} inactivation.

On depolarization of the cell, I_t, I_{sus}, and $I_{Ca,L}$ are also activated. However, I_t and I_{sus} reach their peak magnitude faster than $I_{Ca,L}$, and their combined magnitude is thus larger than that of $I_{Ca,L}$ early in the action potential. (This is because the peak of the action potential is close to the reversal potential for $I_{Ca,L}$.) The initial result on the action potential waveform is therefore a period of relatively rapid repolarization (phase 1), dominated by I_t. Since the time course of inactivation of $I_{Ca,L}$ is slow compared with that of I_t, the net current gradually becomes dominated by $I_{Ca,L}$ and I_{sus}. A situation where the repolarizing effect of I_{sus} (and the remaining I_t) is balanced by the depolarizing effect of $I_{Ca,L}$ results. In the action potential waveform, the initial rapid repolarization (phase 1) is followed by a period during which the membrane potential levels off, forming a plateau (phase 2). Finally, as $I_{Ca,L}$ slowly inactivates, the repolarizing effects of I_{sus} become dominant, and the action potential enters its final repolarization phase (phase 3). During this phase, I_{sus} is aided by the inward rectifier current, I_{K1}, and the delayed rectifier currents, $I_{K,r}$ and $I_{K,s}$, in repolarizing the cell membrane back to the resting potential (phase 4).

Simulated Ionic Fluxes

The fluid compartment part of this model monitors ion concentrations in the intracellular and cleft spaces. Valid modeling of the action potential requires not only the reconstruction of the action potential waveform but also a demonstration that this can be accomplished under conditions of ionic homeostasis at nominal heart rates. Table 4 shows how our model has been tuned to achieve homeostasis at 1 Hz. The average charge transported across the sarcolemma for each ionic current has been computed by integrating each current over one cycle (1 s in the case of a quiescent, nonstimulated cell). Note that the sums of these average charges are zero for all ionic species at a stimulus rate of 1 Hz (Table 4). When the cell is quiescent, there is a small net loss of intracellular Na^+ and gain of intracellular K^+. The existence of such an ionic imbalance at quiescence is supported by the observation by Bénardeau et al[52] that trains of depolarizing pulses that activate I_{Na} can be used to hyperpolarize the resting potential of human atrial cells after a period of quiescence. As suggested by these authors, the hyperpolarization and stabilization of the resting potential may be caused by activation of the Na^+-K^+ pump after Na^+ entry during the train of pulses. In our model, at a 2-Hz stimulus rate there will be a net gain of intracellular Na^+ and loss of K^+.

Fig 9 illustrates the Ca^{2+} handling in the fluid compartment part of the model during the simulated action potential. A transient increase in $[Ca^{2+}]_i$ occurs early in the action potential, raising $[Ca^{2+}]_i$ from the very low diastolic levels (≈65 nmol/L) to a peak of ≈1.3 μmol/L (Fig 9B). This rise in $[Ca^{2+}]_i$ is primarily due to the rapid release of large amounts of Ca^{2+} from the SR (see Fig 9D). Several processes are responsible for the decline of the intracellular Ca^{2+} transient. The most potent of these is the rapid binding of Ca^{2+} to the intracellular Ca^{2+} buffers (troponin and calmodulin), which is particularly important in shaping the early portions of the Ca^{2+} transient. As

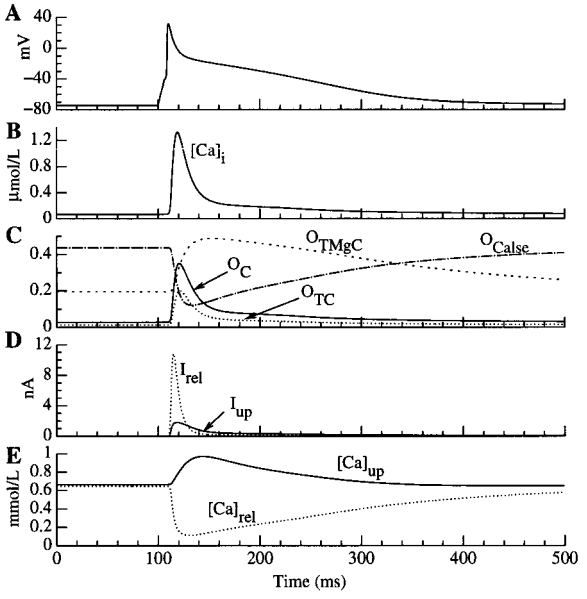

Figure 9. Simulated waveforms for the fluid compartment model. A, Action potential waveform. B, Intracellular Ca^{2+} concentration, $[Ca^{2+}]_i$. C, Occupancies of the troponin (O_{TC} and O_{TMgC}), calmodulin (O_C), and calsequestrin (O_{Calse}) buffers. D, Sarcoplasmic reticulum release and uptake currents (I_{rel} and I_{up}, respectively). E, Ca^{2+} concentrations in the sarcoplasmic reticulum release and uptake compartments ($[Ca^{2+}]_{rel}$ and $[Ca^{2+}]_{up}$, respectively).

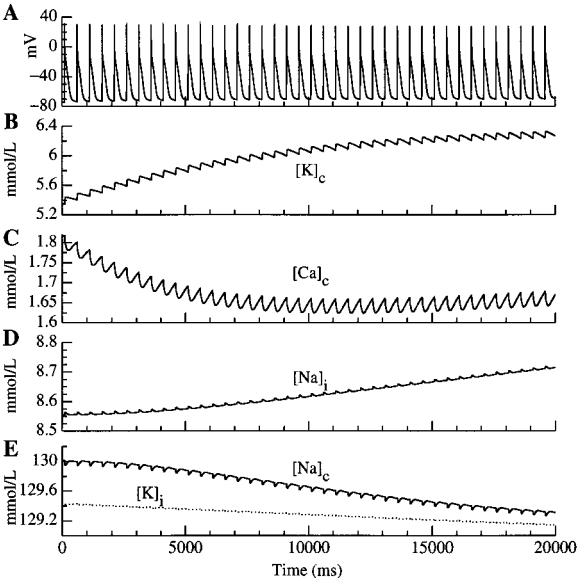

Figure 10. Ion concentrations in the intracellular and cleft spaces when the stimulus rate is increased from 1 to 2 Hz. A, Action potential waveform. B, Cleft space K^+ concentration, $[K^+]_c$. C, Cleft space Ca^{2+} concentration, $[Ca^{2+}]_c$. D, Intracellular Na^+ concentration, $[Na^+]_i$. E, Intracellular K^+ and cleft space Na^+ concentrations, $[K^+]_i$ and $[Na^+]_c$.

seen in Fig 9C, the occupancies on these buffers increase rapidly as Ca^{2+} is released from the SR, thus "removing" large amounts of free Ca^{2+} from the cytosol. The uptake of Ca^{2+} by the SR also has a pronounced effect on the shape of the Ca^{2+} transient. This is also the primary pathway for actual removal of Ca^{2+} from the cytosol (as opposed to the "temporary storage" provided by the buffers), taking up intracellular Ca^{2+} as it dissociates from the buffers. In addition, some Ca^{2+} is removed from the cytosol via the Na^+-Ca^{2+} exchanger, I_{NaCa}, and the Ca^{2+} pump, I_{CaP}. As seen in Table 4, I_{NaCa} and I_{CaP}, on average, remove the amounts of Ca^{2+} that were brought into the cell via $I_{Ca,L}$ and $I_{B,Ca}$ and thereby prevent a progressive buildup of cytosolic Ca^{2+} during repetitive stimulation.

Increasing the stimulus rate from the baseline (1 Hz) results in a change in ion concentrations in the intracellular medium (Table 4) as well as in the cleft space surrounding the cell. For the ionic species that exist in relatively low concentrations in the extracellular medium (Ca^{2+} and K^+), these changes can be significant. Fig 10 shows how the intracellular and cleft space concentrations change when the stimulus rate is increased abruptly from 1 to 2 Hz. Note the progressive shift in $[K^+]_c$ of ≈1 mmol/L.[47,48] In contrast, the change in $[Na^+]_c$ is negligible because of its high baseline value of 130 mmol/L. If the simulation in Fig 10 is continued beyond the 20 s shown, $[K^+]_c$ will reach a peak value of ≈6.3 mmol/L, after which it will begin to decline as a result of increased I_{NaK} activity due to increased $[Na^+]_i$ and $[K^+]_c$ (simulation not shown). The asymptotic values for $[K^+]_c$ and $[Na^+]_i$ are 5.6 and 10.0 mmol/L, respectively (reached after ≈10 minutes). This behavior is consistent with experimental observations.[47]

Parameter Sensitivity of the Action Potential Shape

As mentioned in the previous section, there is considerable variation in action potential shape among individual cells from the human atrium. Our working hypothesis is that many of these differences in action potential waveshape can be explained in terms of differences in the magnitudes of the ionic currents (caused by previous drug treatment and/or natural variability). In order to investigate possible mechanisms of action potential shape variability, it is therefore necessary to have an understanding of how changes in the magnitudes of different ionic currents affect the action potential shape. Such an understanding is equally important, of course, in identifying suitable "targets" for drug action aimed at modifying the action potential shape.

A valid mathematical model provides a method for this sensitivity analysis[53]; ie, it provides a method for studying how sensitive the state variables (eg, membrane voltage) are to perturbations in model parameters. We will restrict this analysis to a study of the sensitivity of the action potential waveform to changes in the sizes (maximum conductances) of the currents involved in shaping the action potential, although this type of analysis in principle can be used to study the sensitivity of any state variable to perturbations in any model parameter. Briefly, sensitivity analysis involves the computation of the partial derivative of the state variable of interest (in this case, membrane voltage) with respect to a model parameter. We have chosen to normalize these partial derivatives with respect to the nominal value of each parameter. Thus, we will present the results in terms of sensitivity functions, defined as:

$$\epsilon_x = \bar{g}_x \frac{\partial v}{\partial \bar{g}_x}$$

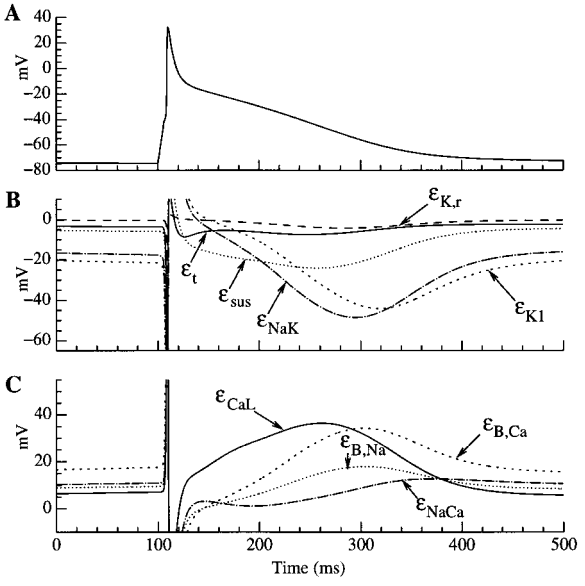

Figure 11. Results of the sensitivity analysis. A, Nominal action potential waveform. B, Sensitivity functions (for the action potential waveform) with respect to scaling factors for outward currents ($\bar{g}_t$, $\bar{g}_{sus}$, $\bar{g}_{K1}$, $\bar{I}_{NaK}$, and $\bar{g}_{K,r}$). C, Sensitivity functions with respect to scaling factors for inward currents ($\bar{g}_{Ca,L}$, $\bar{g}_{B,Na}$, $\bar{g}_{B,Ca}$, and k_{NaCa}).

which can be interpreted as a proportionality factor relating a relative change in a model parameter to a resulting change in membrane voltage. The computational aspects of this method are outlined in Appendix B (see also Paulsen et al[53]).

Fig 11 shows the result of the sensitivity analysis, ie, the sensitivity functions for the membrane voltage (action potential) with respect to the parameters of interest. Sensitivity functions were computed for all maximum conductance parameters in the model as well as for the scaling parameters for I_{NaK} and I_{NaCa}. The sensitivity functions for I_{Na} and $I_{K,s}$ have been omitted from Fig 11, since these currents were found to have negligible influence on the action potential shape (small sensitivity functions), except for the obvious importance of I_{Na} during the upstroke. Several of the sensitivity functions have maximum absolute values of ≈50 mV during the late repolarization phase of the action potential. In other words, a 10% change in either one of these parameters would alter the membrane voltage by ≈5 mV during this phase of the action potential. Although this estimate is based on a linearization around the nominal parameter value and thus is most accurate for small perturbations, it can provide an indication of the approximate change expected for larger perturbations. Overall, we can anticipate that changes in these parameters in the ±50% range will produce significant changes in the action potential waveform.

Perhaps more important than the absolute sensitivity values, however, is the information provided by the time course of the sensitivity functions. As the ionic conductances change during the action potential, the sensitivity functions indicate which currents have the greatest influence on the action potential shape at each point in time. For example, it is clear that the action potential waveform is sensitive to $\bar{g}_t$ primarily early in the peak phase of the action potential but that $\bar{g}_{sus}$ and $\bar{g}_{Ca,L}$ rapidly become more important early in the plateau phase. Throughout the plateau phase, $|\epsilon_{sus}|$ (absolute value) and $|\epsilon_{Ca,L}|$ are larger than $|\epsilon_t|$, and this portion of the action potential waveform is therefore particularly sensitive to perturbations in $\bar{g}_{sus}$ and $\bar{g}_{Ca,L}$. Toward the end of repolarization, the action potential becomes very sensitive to the size of the time-independent currents involved in maintaining the resting potential. This analysis shows that (under the hypothesis that action potential changes can be explained in terms of changes in the magnitudes of ionic currents) $\bar{g}_t$, $\bar{g}_{sus}$, and $\bar{g}_{Ca,L}$ are the most important model parameters in determining the action potential waveshape during the peak and plateau phases of the action potential.

Roles of I_t and I_{sus} in Repolarization

The effects on the human atrial action potential of blocking I_t with agents such as 4-aminopyridine, flecainide, and quinidine have been described in the literature.[2,54–56] Partial block of I_t results in a slowing of the rate of repolarization of the action potential, particularly during the early repolarization phase (phase 1). This is, of course, consistent with the characteristics of I_t, and its role in the generation of the action potential as indicated by sensitivity analysis. In a recent study of the effects of some antiarrhythmic agents on I_t and I_{sus}, Wang et al[56] found that quinidine, in addition to blocking I_t, has a pronounced effect on I_{sus} at clinically relevant concentrations. Considering that our sensitivity analysis indicates a prominent role for I_{sus} in repolarization, the APD is expected to be quite sensitive to modulation of I_{sus} magnitude. A detailed account of the role of I_t and I_{sus} in the repolarization of the human atrial action potential is therefore essential for understanding the antiarrhythmic actions of quinidine.

Since pharmacological blocking agents used in experimental work usually affect more than one current and since their effects are often rate dependent, it is difficult to gain a quantitative understanding of the importance of a particular current (I_t or I_{sus}) in repolarization from experimental results alone. In a computer model, however, it is possible to alter the characteristics of one ionic current in a controlled fashion, while leaving all other currents unaffected. Such simulations can be a valuable complement to experimental work. Given that drugs that prolong the APD (class III drugs) have been shown to be effective in the treatment of atrial arrhythmias,[57] a thorough understanding of the influence of different ionic currents on the APD is needed.

Fig 12A shows the effects on the action potential of various degrees (30%, 60%, and 90%) of block of I_t. (In the present study, an x% block of I_t is simulated as an x% reduction in the maximum conductance, $\bar{g}_t$.) As observed experimentally, I_t block results in a broadening of the action potential peak during phase 1 of repolarization (refer to Fig 2 in Firek and Giles[2]). In addition, because of the elevation of the action potential peak and plateau levels, the contribution of I_{sus} to repolarization is increased. The resulting prolongation of the APD is therefore only moderate, even for substantial reductions of I_t size. Fig 12B shows the effects of various degrees (15%, 30%, and 45%) of block of I_{sus} on the action potential. In contrast to I_t block, inhibition of I_{sus} primarily affects the plateau phase of the action potential, with little or no effect on

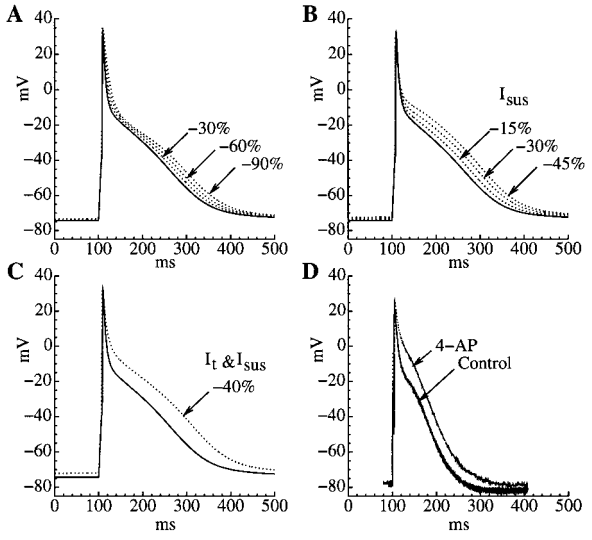

Figure 12. Effects of partial block of I_t and I_{sus}. A, I_t block (30%, 60%, and 90%) has its main effect on the peak and produces only a moderate prolongation of the action potential. B, I_{sus} block (15%, 30%, and 45%) has a strong effect on the action potential duration. C, Combined block (40%) of I_t and I_{sus} widens the peak and prolongs the action potential, in a way similar to the effect of 4-aminopyridine (4-AP). D, Recorded action potential under control conditions and in the presence of 4-AP (data from Firek and Giles[2]).

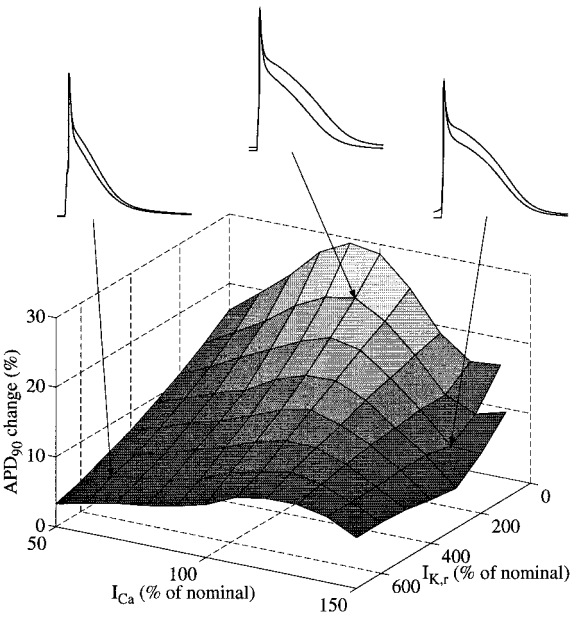

Figure 13. Prolongation of action potential duration at 90% repolarization (APD_{90}) as a result of 50% reduction of I_{sus} size, plotted as a function of the baseline $I_{Ca,L}$ and $I_{K,r}$ sizes. (100% denotes the nominal sizes of $I_{Ca,L}$ and $I_{K,r}$.) Insets show examples of action potentials (before and after I_{sus} block) corresponding to three points in the graph (middle inset is for the nominal model).

the action potential peak. As a result, I_{sus} block produces a more pronounced prolongation of the APD than does I_t block. For example, 30% block of I_{sus} results in a 15% increase in APD at 90% repolarization (APD_{90}) compared with the 5% increase in APD_{90} resulting from 30% I_t block. Many antiarrhythmic agents have effects on several ion channels. For example, according to Wang et al,[56] quinidine blocks both I_t and I_{sus} (in addition to its effects on Na^+ channels). It is therefore of interest to study the effects on the action potential of combined I_t and I_{sus} block. Fig 12C shows the result of a simulation in which both I_t and I_{sus} have been reduced by 40% (approximately corresponding to the effect of 5 μmol/L quinidine at a stimulus rate of 1 Hz[56]). As expected, the result is essentially a combination of the previously demonstrated effects of I_t and I_{sus} block, ie, a widened peak, an elevated action potential plateau, and a prolongation of APD_{90} of 27%.

Modulation of the Role of I_{sus} by Baseline $I_{Ca,L}$, I_{sus}, and $I_{K,r}$ Sizes

As discussed in "Model Development," published data regarding the size of $I_{Ca,L}$ and I_{sus} are quite variable. Both these currents (as well as I_t) are known to be depressed in diseased human atrial cells[22,26] and modulated by adrenergic stimulation.[26,58] Furthermore, a recent study[59] shows that the size of I_{sus} is significantly reduced in cells obtained from patients in chronic atrial fibrillation compared with patients in normal sinus rhythm. It is therefore likely that a range of sizes of these two currents contributes to the physiological (and pathophysiological) behavior of the human atrial cell. Similarly, $I_{K,r}$ in our nominal model is very small, which is consistent with observations from our laboratory. Since results in other species[60] indicate that this may be a consequence of the cell isolation techniques used for human atrial myocytes,[2] this current may be considerably larger in vivo. Given these uncertainties in the actual sizes of several of the ionic currents, it is appropriate to investigate how the conclusions reached above are affected by our assumptions for these current sizes. We have chosen to focus on the role of I_{sus} in repolarization, since this current is an important determinant of APD. Starting from our nominal model, we have performed a large number of simulations for different combinations of increased/decreased $I_{Ca,L}$, I_{sus}, and $I_{K,r}$. All simulations were performed at a stimulation rate of 1 Hz, and 20 cycles were allowed after each change of parameter values in order for any initial transient behavior to die out before the APD prolongation was evaluated. Fig 13 shows how the APD prolongation resulting from a 50% reduction of I_{sus} depends on the baseline sizes of $I_{Ca,L}$ and $I_{K,r}$. $I_{Ca,L}$ and $I_{K,r}$ sizes are expressed as percentages of those in the nominal model; ie, the nominal model corresponds to 100% of both currents. A 7-fold (700%) increase in $I_{K,r}$ corresponds approximately to the size of $I_{K,r}$ observed in rabbit atrial myocytes.[41] It is clear from Fig 13 that the role of I_{sus} as a major determinant of APD depends strongly on the size of $I_{K,r}$ current. The action potentials shown in the insets in Fig 13 provide an indication of the underlying mechanism. When I_{sus} is partially blocked, the action potential plateau is depolarized, which in turn increases the amount of $I_{K,r}$ (and $I_{K,s}$) that is activated. This effect, which counteracts the APD-prolonging effect of I_{sus} block, becomes stronger as the size of $I_{K,r}$ is increased. Similarly, Fig 14 shows how the APD prolongation as a result of 50% I_{sus} block depends on the baseline sizes of $I_{Ca,L}$ and I_{sus}. Again, the APD-prolonging effect of I_{sus} block is strongly dependent on the baseline current densities. Generally, the APD prolongation as a result of partial I_{sus} block becomes larger as the baseline size of $I_{Ca,L}$ increases, provided that the increase

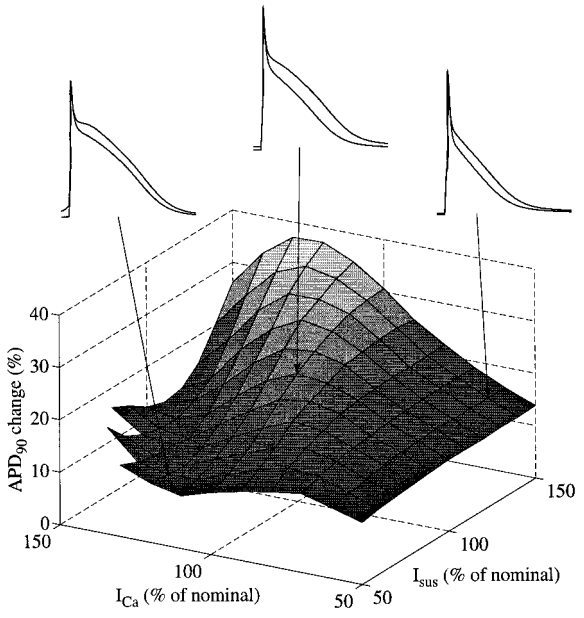

Figure 14. Prolongation of action potential duration at 90% repolarization (APD_{90}) as a result of 50% reduction of I_{sus} size, plotted as a function of the baseline $I_{Ca,L}$ and I_{sus} sizes. Insets show examples of action potentials (before and after I_{sus} block) corresponding to three points in the graph (middle inset is for the nominal model).

in $I_{Ca,L}$ is balanced by a comparable increase in I_{sus}. Notice, however, in Fig 13 as well as in Fig 14, that when baseline $I_{Ca,L}$ is increased without such a comparable increase in baseline outward current (I_{sus} or $I_{K,r}$), the APD-prolonging effect of I_{sus} block is instead reduced. The underlying mechanism in this case is that the action potential plateau, both before and after I_{sus} block, is prolonged and depolarized somewhat by the larger $I_{Ca,L}$. As a result, more $I_{K,r}$ (and $I_{K,s}$) is activated, and the final repolarization phase becomes steeper and therefore less dependent on I_{sus}.

Discussion

Mathematical models form an important complement to experimental work in attempts to elucidate the ionic mechanisms underlying the action potential and other electrophysiological phenomena in cardiac cells. At a minimum, these models can provide a means of integrating data obtained from many different experiments and laboratories so that biophysically based explanations of complex nonlinear phenomena such as action potential initiation (excitation) and repolarization can be given. Mathematical models also provide a way of reviewing data in the context of the normal behavior of a cell (during an action potential), even when some of the data may have been obtained under completely different experimental conditions, eg, a voltage-clamp experiment. Moreover, as illustrated in the last few sections of "Results," mathematical models can also have considerable predictive capabilities. After a model has been developed and carefully validated, it can be used to predict the response of the cell to selected drugs, experimental protocols, etc. Ideally, experimental work and model development should be carried out in close association, using the model to design and evaluate experiments and using experimental results to improve the model.

We have developed a mathematical model of the human atrial cell based primarily on data recorded from enzymatically isolated single human atrial cells. Our model is capable of accurately reconstructing a recorded human atrial action potential and illustrates the functional roles of the ionic currents. In addition, our model maintains ionic homeostasis at a nominal stimulus rate, demonstrating that the reconstruction of the action potential is accomplished using plausible current densities. We used the LMCG rabbit atrial model[13] as a "starting point" for the model development. As a result, these two formulations are very similar in some aspects, particularly for the membrane currents where incomplete (or no) data from human atrial cells are available. However, there are some important differences between the electrophysiological responses of rabbit and human atrial cells; these provided the motivation for the development of this human atrial cell model. Perhaps most striking is the small rate dependence of I_t in human atrial cells compared with the very prominent rate dependence seen in rabbit atrial cells.[13,38] This is mainly due to differences in the rates of recovery from inactivation of I_t in the two species. As discussed in "Membrane Currents," I_t in human atrial cells recovers from inactivation much more rapidly than does I_t in rabbit atrial cells. Another important difference between human and rabbit atrial cells is the sustained outward current (denoted I_{sus} in this article). Whereas this current in the rabbit atrium is believed to be carried mainly by Cl^- ions,[13] there is convincing evidence that I_{sus} in human atrial cells is carried mainly by K^+ ions.[2,35] Both these differences are very important in studying the mechanisms of repolarization of the human atrial action potential and the effects of action potential–prolonging (class III) drugs that affect these currents.

Roles of I_t and I_{sus} in Repolarization

Both I_t and I_{sus} have important roles in the repolarization of the action potential of human atrium. In particular, I_{sus}, because of its noninactivating characteristics, is necessary for repolarization to the resting potential. This important role in repolarization makes I_t and I_{sus} potential targets for class III antiarrhythmic drugs, which are designed to prolong the APD. Indeed, a recent study of flecainide and quinidine,[56] both known to prolong the human atrial action potential,[54,55] shows that both these drugs produce a partial block of I_t. Quinidine also blocks I_{sus}, which could explain its greater efficacy (compared with flecainide) in prolonging the APD.[55] Our simulations of partial I_t and I_{sus} block (see "Results") produce prolongations of the APD that are comparable to experimentally observed effects of flecainide and quinidine, ie, a 27% prolongation of APD_{90} when I_t and I_{sus} are both reduced by 40%. For comparison, Wang et al[55] reported that 2.25 μmol/L quinidine increased APD_{95} by 33% in human atrial cells at a stimulation rate of 1 Hz. It should be noted that only some of the known effects of quinidine have been modeled; therefore, our results cannot be directly compared with these experimental observations. For example, the effects of quinidine on I_{Na}, as well as the state dependence of I_t block by quinidine,[61] would have to be included in a more comprehensive treatment of quinidine effects. Nevertheless, the experimental observations

agree very well with our model predictions and provide an independent "test" of how well our model describes the roles of I_t and I_{sus} in repolarization.

Action potential generation involves a complex interaction among the ionic currents in a given cell type. The role of a particular ionic current in the action potential is therefore not determined solely by the characteristics of that current. We have investigated how the role of I_{sus} in repolarization is affected when the baseline densities of $I_{Ca,L}$, I_{sus}, and $I_{K,r}$ are varied within ranges that are relevant to the physiological and pathophysiological behavior of the human atrial cell. Our results demonstrate that I_{sus} block will, in general, result in a prolongation of the action potential. The amount of prolongation, however, depends quite strongly on the baseline current densities. If the human atrial cell is assumed to have an $I_{K,r}$ density comparable to that observed in the rabbit atrium[41] or if the $I_{Ca,L}$ and I_{sus} densities are reduced as observed in diseased cells,[22,26] the APD prolongation resulting from I_{sus} block may be considerably smaller than indicated by our nominal model. The efficacy of a drug targeting I_{sus} would therefore be expected to depend critically on the disease state of the tissue. For example, based on the recent observation by Van Wagoner et al[59] that I_{sus} density is reduced in cells obtained from patients in chronic atrial fibrillation, the efficacy of an I_{sus}-blocking drug may be limited in these patients.

Limitations of the Model

When using our model to gain insight into the electrophysiological responses of the human atrial cell, it is important to be aware of certain limitations, which are summarized by the following items:

1. The Hodgkin-Huxley formalism along with its concept of independent activation and inactivation "gating" variables has some important limitations. Notably, the processes of inactivation and recovery from inactivation (and analogously activation and deactivation) are governed by a single time constant. Experimental observations, however, often indicate that inactivation and recovery from inactivation occur with different time constants, even at the same membrane potential. In order to overcome this problem, one would have to use a more complicated modeling formalism that treats inactivation and recovery as two separate processes. To reduce the computational requirements of the model, we have chosen a "compromise" solution, in which time constant values are determined by measured inactivation kinetics at depolarized membrane potentials and by measured recovery kinetics at hyperpolarized potentials. In cases in which the time constants of inactivation and recovery are very different, this compromise results in unconventional time constant expressions, such as those for I_{Na} in Fig 2D.

2. The available data regarding the intracellular Ca^{2+} transient and the Ca^{2+} handling in the SR have, with few exceptions,[52,62] been recorded in cells from species other than humans. In addition, the understanding of the exact mechanisms involved in these phenomena is incomplete, and a quantitative model of SR Ca^{2+} release and uptake has not yet been developed. Our Ca^{2+}-dependent formulation for SR Ca^{2+} release replaces the voltage-dependent formulation used in earlier models[4,12,13] but is nevertheless only a qualitative description of this phenomenon. Other features of the SR function are the same as those in the LMCG model.[13] Our SR formulation is therefore not based on human data.

3. The shape of the action potentials recorded from enzymatically isolated human atrial cells is variable, even at a fixed stimulus frequency. There are several reasons for this variability, including genuine heterogeneity between cells from different parts of the atrium, the disease states of the patients from whom the specimens are obtained, and the use of various drugs (eg, Ca^{2+} channel blockers and β-blockers) by the donors. It is important to acknowledge that this variability exists and that the exact action potential waveform in the model is chosen because it is representative of the action potential shapes that are most often observed in our single cell records. As indicated by sensitivity analysis, the shape of the human atrial action potential as described by our model is quite sensitive to variations in the strengths of three ionic currents (I_t, I_{sus}, and $I_{Ca,L}$). Under the assumption that the currents involved and their kinetic properties are unchanged, our results therefore suggest that the experimentally observed variation in action potential shape is caused mainly by variations in these currents and can be explained within the framework of our model. However, it is also conceivable that regional diversity in the molecular basis of the currents in human atrium could give rise to regional differences in kinetics and pharmacological sensitivity. Most of the data on human atrial electrophysiology to date have been obtained from samples of the atrial appendage, and there are therefore little experimental data available regarding regional differences in human atrium. If and when data to suggest regional diversity become available, our model should provide a useful framework for predicting the consequences.

4. Our model of Ca^{2+}-dependent inactivation of $I_{Ca,L}$ uses a single lumped subsarcolemmal compartment in which Ca^{2+} accumulates and is therefore limited in its ability to simulate the effect of Ca^{2+} accumulation in restricted spaces close to each L-type Ca^{2+} channel. In contrast to voltage-dependent gating, where it is reasonable to assume that the controlling variable (membrane voltage) is spatially uniform (space-clamp conditions), this is in all likelihood not the case for subsarcolemmal Ca^{2+}. Since inactivation is a nonlinear function of $[Ca^{2+}]_d$, it is not strictly correct to use a formulation in which all channels are subject to one (average) Ca^{2+} concentration.

Notwithstanding these limitations, this model provides the most complete description available of the ionic mechanisms underlying the human atrial action potential, and it is based on the available data. As a result, it provides a very useful tool for investigating fundamental electrophysiological responses of the human atrial cell, such as excitability, refractoriness, and the action of channel blocking drugs.

Appendix 1: Model Equations

Tables 5 through 19 contain all the equations, parameter values, and initial conditions necessary to carry out the simulations presented in this article. Unless otherwise noted, the units are as follows: time in seconds (s), voltage in millivolts (mV), concentration in millimoles/liter (mmol/L), current in picoamperes (pA), conductance in nanosiemens (nS), capacitance in nanofarads (nF), volume in nanoliters (nL), and temperature in kelvin (K). The stimulus used to evoke an action potential consists of a rectangular current pulse (I_{stim}) with an amplitude of 280 pA and duration of 6 ms.

TABLE 5. Membrane Voltage: V

$$\frac{dV}{dt} = \frac{I_{Na} + I_{Ca,L} + I_t + I_{sus} + I_{K1} + I_{B,Na} + I_{B,Ca} + I_{NaK} + I_{CaP} + I_{NaCa} - I_{stim}}{-C_m}$$

TABLE 6. Na^+ Current: I_{Na}

$$I_{Na} = P_{Na} m^3 (0.9h_1 + 0.1h_2)[Na^+]_c V \frac{F^2}{RT} \frac{e^{(V-E_{Na})F/RT} - 1.0}{e^{VF/RT} - 1.0}$$

$$\bar{m} = \frac{1.0}{1.0 + e^{(V+27.12)/-8.21}} \qquad \bar{h} = \frac{1.0}{1.0 + e^{(V+63.6)/5.3}}$$

$$\frac{dm}{dt} = \frac{\bar{m} - m}{\tau_m} \qquad \tau_m = 0.000042e^{-((v+25.57)/28.8)^2} + 0.000024$$

$$\frac{dh_1}{dt} = \frac{\bar{h} - h_1}{\tau_{h_1}} \qquad \tau_{h_1} = \frac{0.03}{1.0 + e^{(V+35.1)/3.2}} + 0.0003$$

$$\frac{dh_2}{dt} = \frac{\bar{h} - h_2}{\tau_{h_2}} \qquad \tau_{h_2} = \frac{0.12}{1.0 + e^{(V+35.1)/3.2}} + 0.003$$

$$E_{Na} = \frac{RT}{F} \log \frac{[Na^+]_c}{[Na^+]_i}$$

TABLE 7. Ca^{2+} Current: $I_{Ca,L}$

$$I_{Ca} = \bar{g}_{Ca,L} d_L [f_{Ca} f_{L_1} + (1 - f_{Ca}) f_{L_2}](V - E_{Ca,app})$$

$$\bar{d}_L = \frac{1.0}{1.0 + e^{(V+9.0)/-5.8}} \qquad \bar{f}_L = \frac{1.0}{1.0 + e^{(V+27.4)/7.1}}$$

$$\frac{dd_L}{dt} = \frac{\bar{d}_L - d_L}{\tau_{d_L}} \qquad \tau_{d_L} = 0.0027e^{-((v+35.0)/30.0)^2} + 0.002$$

$$\frac{df_{L_1}}{dt} = \frac{\bar{f}_L - f_{L_1}}{\tau_{f_{L_1}}} \qquad \tau_{f_{L_1}} = 0.161e^{-((V+40.0)/14.4)^2} + 0.010$$

$$\frac{df_{L_2}}{dt} = \frac{\bar{f}_L - f_{L_2}}{\tau_{f_{L_2}}} \qquad \tau_{f_{L_2}} = 1.3323e^{-((V+40.0)/14.2)^2} + 0.0626$$

$$f_{Ca} = \frac{[Ca^{2+}]_d}{[Ca^{2+}]_d + k_{Ca}}$$

TABLE 8. Transient and Sustained Outward K^+ Currents: I_t and I_{sus}

$$I_t = \bar{g}_t r s (V - E_K)$$

$$\bar{r} = \frac{1.0}{1.0 + e^{(V-1.0)/-11.0}} \qquad \bar{s} = \frac{1.0}{1.0 + e^{(V+40.5)/11.5}}$$

$$\frac{dr}{dt} = \frac{\bar{r} - r}{\tau_r} \qquad \tau_r = 0.0035 e^{-(V/30.0)^2} + 0.0015$$

$$\frac{ds}{dt} = \frac{\bar{s} - s}{\tau_s} \qquad \tau_s = 0.4812 e^{-((V+52.45)/14.97)^2} + 0.01414$$

$$I_{sus} = \bar{g}_{sus} r_{sus} s_{sus} (V - E_K)$$

$$\bar{r}_{sus} = \frac{1.0}{1.0 + e^{(V+4.3)/-8.0}} \qquad \bar{s}_{sus} = \frac{0.4}{1.0 + e^{(V+20.0)/10.0}} + 0.6$$

$$\frac{dr_{sus}}{dt} = \frac{\bar{r}_{sus} - r_{sus}}{\tau_{r_{sus}}} \qquad \tau_{r_{sus}} = \frac{0.009}{1.0 + e^{(V+5.0)/12.0}} + 0.0005$$

$$\frac{ds_{sus}}{dt} = \frac{\bar{s}_{sus} - s_{sus}}{\tau_{s_{sus}}} \qquad \tau_{s_{sus}} = \frac{0.047}{1.0 + e^{(V+60.0)/10.0}} + 0.300$$

$$E_K = \frac{RT}{F} \log \frac{[K^+]_c}{[K^+]_i}$$

TABLE 9. Delayed Rectifier K^+ Currents: $I_{K,s}$ and $I_{K,r}$

$$I_{K,s} = \bar{g}_{K,s} n (V - E_K)$$

$$\bar{n} = \frac{1.0}{1.0 + e^{(V-19.9)/-12.7}} \qquad \tau_n = 0.7 + 0.4 e^{-((V-20.0)/20.0)^2}$$

$$\frac{dn}{dt} = \frac{\bar{n} - n}{\tau_n} \qquad E_K = \frac{RT}{F} \log \frac{[K^+]_c}{[K^+]_i}$$

$$I_{K,r} = \bar{g}_{K,r} p_a p_i (V - E_K)$$

$$\bar{p}_a = \frac{1.0}{1.0 + e^{(V+15.0)/-6.0}} \qquad p_i = \frac{1.0}{1.0 + e^{(V+55.0)/24.0}}$$

$$\frac{dp_a}{dt} = \frac{\bar{p}_a - p_a}{\tau_{p_a}} \qquad \tau_{p_a} = 0.03118 + 0.21718 e^{-((V+20.1376)/22.1996)^2}$$

TABLE 10. Inward Rectifier K^+ Current: I_{K1}

$$I_{K1} = \bar{g}_{K1} [K^+]_c^{0.4457} \frac{V - E_K}{1.0 + e^{1.5(V-E_K+3.6)F/RT}}$$

$$E_K = \frac{RT}{F} \log \frac{[K^+]_c}{[K^+]_i}$$

TABLE 11. Background Inward Currents: $I_{B,Na}$ and $I_{B,Ca}$

$$I_{B,Na} = \bar{g}_{B,Na} (V - E_{Na}) \qquad I_{B,Ca} = \bar{g}_{B,Ca} (V - E_{Ca})$$

$$E_{Na} = \frac{RT}{F} \log \frac{[Na^+]_c}{[Na^+]_i} \qquad E_{Ca} = \frac{RT}{2F} \log \frac{[Ca^{2+}]_c}{[Ca^{2+}]_i}$$

TABLE 12. Pump and Exchanger Currents: I_{NaK}, I_{CaP}, and I_{NaCa}

$$I_{NaK} = \bar{I}_{NaK} \frac{[K^+]_c}{[K^+]_c + k_{NaK,K}} \cdot \frac{[Na^+]_i^{1.5}}{[Na^+]_i^{1.5} + k_{NaK,Na}^{1.5}} \cdot \frac{V + 150.0}{V + 200.0}$$

$$I_{CaP} = \bar{I}_{CaP} \frac{[Ca^{2+}]_i}{[Ca^{2+}]_i + k_{CaP}}$$

$$I_{NaCa} = k_{NaCa} \frac{[Na^+]_i^3[Ca^{2+}]_c e^{\gamma VF/RT} - [Na^+]_c^3[Ca^{2+}]_i e^{(\gamma-1.0)VF/RT}}{1.0 + d_{NaCa}([Na^+]_c^3[Ca^{2+}]_i + [Na^+]_i^3[Ca^{2+}]_c)}$$

TABLE 13. Intracellular Ion Concentrations: $[Na^+]_i$, $[K^+]_i$, and $[Ca^{2+}]_i$

$$\frac{d[Na^+]_i}{dt} = -\frac{I_{Na} + I_{B,Na} + 3I_{NaK} + 3I_{NaCa} + \Phi_{Na,en}}{Vol_i F}$$

$$\frac{d[K^+]_i}{dt} = -\frac{I_t + I_{sus} + I_{K1} + I_{K,s} + I_{K,r} - 2I_{NaK}}{Vol_i F}$$

$$\frac{d[Ca^{2+}]}{dt} = -\frac{-I_{di} + I_{B,Ca} + I_{CaP} - 2I_{NaCa} + I_{up} - I_{rel}}{2.0\ Vol_i F} - \frac{dO}{dt}$$

$$\frac{dO}{dt} = 0.08 \frac{dO_{TC}}{dt} + 0.16 \frac{dO_{TMgC}}{dt} + 0.045 \frac{dO_C}{dt}$$

$$\frac{d[Ca^{2+}]_d}{dt} = -\frac{I_{Ca,L} - I_{di}}{2.0\ Vol_d F}$$

$$I_{di} = ([Ca^{2+}]_d - [Ca^{2+}]_i) \frac{2F\ Vol_d}{\tau_{di}}$$

TABLE 14. Cleft Space Ion Concentrations: $[Na^+]_c$, $[K^+]_c$, and $[Ca^{2+}]_c$

$$\frac{d[Na^+]_c}{dt} = \frac{[Na^+]_b - [Na^+]_c}{\tau_{Na}} + \frac{I_{Na} + I_{B,Na} + 3I_{NaK} + 3I_{NaCa} + \Phi_{Na,en}}{Vol_c F}$$

$$\frac{d[K^+]_c}{dt} = \frac{[K^+]_b - [K^+]_c}{\tau_K} + \frac{I_t + I_{sus} + I_{K1} + I_{K,s} + I_{K,r} - 2I_{NaK}}{Vol_c F}$$

$$\frac{d[Ca^{2+}]_c}{dt} = \frac{[Ca^{2+}]_b - [Ca^{2+}]_c}{\tau_{Ca}} + \frac{I_{Ca,L} + I_{B,Ca} + I_{CaP} - 2I_{NaCa}}{2.0\ Vol_c F}$$

TABLE 15. Intracellular Ca^{2+} Buffering

$$\frac{dO_C}{dt} = 200000.0[Ca^{2+}]_i(1.0 - O_C) - 476.0O_C$$

$$\frac{dO_{TC}}{dt} = 78400.0[Ca^{2+}]_i(1.0 - O_{TC}) - 392.0O_{TC}$$

$$\frac{dO_{TMgC}}{dt} = 200000.0[Ca^{2+}]_i(1.0 - O_{TMgC} - O_{TMgMg}) - 6.6O_{TMgC}$$

$$\frac{dO_{TMgMg}}{dt} = 2000.0[Mg^{2+}]_i(1.0 - O_{TMgC} - O_{TMgMg}) - 666.0O_{TMgMg}$$

TABLE 16. Ca^{2+} Handling by the Sarcoplasmic Reticulum

$$I_{up} = \bar{I}_{up} \frac{[Ca^{2+}]_i/k_{cyca} - k_{xcs}^2[Ca^{2+}]_{up}/k_{srca}}{([Ca^{2+}]_i + k_{cyca})/k_{cyca} + k_{xcs}([Ca^{2+}]_{up} + k_{srca})/k_{srca}}$$

$$I_{tr} = ([Ca^{2+}]_{up} - [Ca^{2+}]_{rel}) \frac{2F\ Vol_{rel}}{\tau_{tr}}$$

$$I_{rel} = \alpha_{rel} \left(\frac{F_2}{F_2 + 0.25}\right)^2 ([Ca^{2+}]_{rel} - [Ca^{2+}]_i)$$

$$\frac{dO_{Calse}}{dt} = 480.0[Ca^{2+}]_{rel}(1.0 - O_{Calse}) - 400.0O_{Calse}$$

$$\frac{d[Ca^{2+}]_{rel}}{dt} = \frac{I_{tr} - I_{rel}}{2\ Vol_{rel} F} - 31.0\frac{dO_{Calse}}{dt}$$

$$\frac{d[Ca^{2+}]_{up}}{dt} = \frac{I_{up} - I_{tr}}{2\ Vol_{up} F}$$

$$\frac{dF_1}{dt} = r_{recov}(1.0 - F_1 - F_2) - r_{act}F_1$$

$$\frac{dF_2}{dt} = r_{act}F_1 - r_{inact}F_2$$

$$r_{act} = 203.8\left\{\left(\frac{[Ca^{2+}]_i}{[Ca^{2+}]_i + k_{rel,i}}\right)^4 + \left(\frac{[Ca^{2+}]_d}{[Ca^{2+}]_d + k_{rel,d}}\right)^4\right\}$$

$$r_{inact} = 33.96 + 339.6\left(\frac{[Ca^{2+}]_i}{[Ca^{2+}]_i + k_{rel,i}}\right)^4$$

TABLE 17. Parameter Values

$[Na^+]_b$=130.0 mmol/L	$\bar{I}_{NaK}$=70.8253 pA
$[K^+]_b$ =5.4 mmol/L	$k_{NaK,K}$=1.0 mmol/L
$[Ca^{2+}]_b$ =1.8 mmol/L	$k_{NaK,Na}$=11.0 mmol/L
$[Mg^{2+}]_i$=2.5 mmol/L	$\bar{I}_{CaP}$=4.0 pA
$E_{Ca,app}$=60.0 mV	k_{CaP}=0.0002 mmol/L
k_{Ca}=0.25 mmol/L	k_{NaCa}=0.0374842 pA/(mmol/L)^4
R=8314.0 mJ/molK	γ=0.45
T=306.15 K (=33°C)	d_{NaCa}=0.0003 (mmol/L)$^{-4}$
F=96487.0 C/mol	$\Phi_{Na,en}$=−1.68 pA
C_m=0.05 nF	$\bar{I}_{up}$=2800.0 pA
Vol_c=0.136 Vol_i	k_{cyca}=0.0003 mmol/L
Vol_i=0.005884 nL	k_{srca}=0.5 mmol/L
Vol_d=0.02 Vol_i	k_{xcs}=0.4
Vol_{rel}=0.0000441 nL	τ_{tr}=0.01 s
Vol_{up}=0.0003969 nL	α_{rel}=200000.0 pA L/mmol
τ_{Na}=14.3 s	$k_{rel,i}$=0.0003 mmol/L
τ_K=10.0 s	$k_{rel,d}$=0.003 mmol/L
τ_{Ca}=24.7 s	r_{recov}=0.815 s^{-1}
τ_{dt}=0.010 s	

TABLE 18. Maximum Conductance Values

P_{Na}=0.0016 nL/s	$\bar{g}_{K,r}$=0.5 nS
$\bar{g}_{Ca,L}$=6.75 nS	$\bar{g}_{K1}$=3.0 nS
$\bar{g}_t$=7.5 nS	$\bar{g}_{B,Na}$=0.060599 nS
$\bar{g}_{sus}$=2.75 nS	$\bar{g}_{B,Ca}$=0.078681 nS
$\bar{g}_{K,s}$=1.0 nS	

TABLE 19. Initial Conditions

V=−74.2525 mV	f_{L_2}=0.9986
$[Na^+]_c$=130.0110 mmol/L	r=1.0678×10^{-3}
$[K^+]_c$=5.3581 mmol/L	s=0.9490
$[Ca^{2+}]_c$=1.8147 mmol/L	r_{sus}=1.5949×10^{-4}
$[Na^+]_i$=8.5547 mmol/L	s_{sus}=0.9912
$[K^+]_i$=129.4350 mmol/L	n=4.8357×10^{-3}
$[Ca^{2+}]_i$=6.7290×10^{-5} mmol/L	p_a=0.0001
$[Ca^{2+}]_d$=7.2495×10^{-5} mmol/L	F_1=0.4284
$[Ca^{2+}]_{up}$=0.6646 mmol/L	F_2=0.0028
$[Ca^{2+}]_{rel}$=0.6465 mmol/L	O_C=0.0275
m=3.2017×10^{-3}	O_{TC}=0.0133
h_1=0.8814	O_{TMgC}=0.1961
h_2=0.8742	O_{TMgMg}=0.7094
d_L=1.3005×10^{-5}	O_{Calse}=0.4369
f_{L_1}=0.9986	

All simulations were performed by forward integration of the coupled system of differential equations using the CVODE solver package for ordinary differential equations. (CVODE was developed by S.D. Cohen and A.C. Hindmarsh at Lawrence Livermore National Laboratories, Livermore Calif) Sufficient accuracy was ensured by adjusting the temporal step size of the integration so that the local error in all state variables (as estimated by the CVODE algorithm) satisfied a relative error bound. Computer programs for the simulations were written in the C programming language under the UNIX operating system. Simulations were performed on Sun Microsystems Sparc workstations (Sparc 2, IPX) and on a Micron Millennia Pentium 166 PC running the Linux operating system. At a stimulus frequency of 1 Hz, one cycle (ie, 1 s of data) requires ≈0.9 s of CPU time on the Pentium 166 platform.

Appendix 2: Sensitivity Analysis

This Appendix contains a brief derivation of the method used to study the parameter sensitivity of the action potential waveform. The reader is referred to Reference 53 for more detailed information.

Starting from a system of the general form,

$$\frac{\mathrm{d}}{\mathrm{dt}}\mathbf{x} = \mathbf{f}(\alpha, \mathbf{x}, \mathrm{t})$$

we take the partial derivative of Equation 1 with respect to a parameter α_k to obtain the following equation:

$$\frac{\partial}{\partial \alpha_k}\left\{\frac{\mathrm{d}}{\mathrm{dt}}\mathbf{x}\right\} = \frac{\partial}{\partial \alpha_k}\mathbf{f}(\alpha, \mathbf{x}, \mathrm{t}) =$$

$$\begin{bmatrix} \frac{\partial f_1}{\partial x_1} & \cdots & \frac{\partial f_1}{\partial x_N} \\ \vdots & \ddots & \vdots \\ \frac{\partial f_N}{\partial x_1} & \cdots & \frac{\partial f_N}{\partial x_N} \end{bmatrix} \begin{bmatrix} \frac{\partial x_1}{\partial \alpha_k} \\ \vdots \\ \frac{\partial x_N}{\partial \alpha_k} \end{bmatrix} + \begin{bmatrix} \frac{\partial f_1}{\partial \alpha_k} \\ \vdots \\ \frac{\partial f_N}{\partial \alpha_k} \end{bmatrix} =$$

$$\mathrm{J}_{\mathbf{x}}^{\mathbf{f}}\frac{\partial \mathbf{x}}{\partial \alpha_k} + \frac{\partial \mathbf{f}}{\partial \alpha_k}$$

The time derivative of the state vector $\mathbf{x}(\alpha, t)$ can be written as follows:

$$\frac{\mathrm{d}}{\mathrm{dt}}\mathbf{x}(\alpha, \mathrm{t}) = \mathrm{J}_{\alpha}^{\mathbf{x}}\frac{\partial \alpha}{\partial \mathrm{t}} + \frac{\partial \mathbf{x}(\alpha, \mathrm{t})}{\partial \mathrm{t}} = \frac{\partial}{\partial \mathrm{t}}\mathbf{x}(\alpha, \mathrm{t})$$

where the time derivative of α vanishes, since all parameters are assumed to be time invariant. Thus, from Equation 1, we have the following:

$$\frac{\partial}{\partial \alpha_k}\left\{\frac{\partial}{\partial \mathrm{t}}\mathbf{x}\right\} = \mathrm{J}_{\mathbf{x}}^{\mathbf{f}}\frac{\partial \mathbf{x}}{\partial \alpha_k} + \frac{\partial \mathbf{f}}{\partial \alpha_k}$$

Interchanging the order of integration, we obtain the following equation:

$$\frac{\partial}{\partial \mathrm{t}}\left\{\frac{\partial}{\partial \alpha_k}\mathbf{x}\right\} = \frac{\partial}{\partial \mathrm{t}}\boldsymbol{\epsilon}_k = \mathrm{J}_{\mathbf{x}}^{\mathbf{f}}\frac{\partial \mathbf{x}}{\partial \alpha_k} + \frac{\partial \mathbf{f}}{\partial \alpha_k}$$

where $\boldsymbol{\epsilon}_k$ is the sensitivity of the state $\mathbf{x}$ to the parameter α_k, ie,

$$\boldsymbol{\epsilon}_k = \frac{\partial}{\partial \alpha_k}\mathbf{x}$$

Note, finally, that Equation 5 defines a costate system[53] of the same general form as Equation 1, ie,

$$\frac{\partial}{\partial \mathrm{t}}\boldsymbol{\epsilon}_k = \mathbf{f}_k(\alpha, \mathbf{x}, \mathrm{t})$$

where

$$\mathbf{f}_k(\alpha, \mathbf{x}, \mathrm{t}) = \mathrm{J}_{\mathbf{x}}^{\mathbf{f}}\frac{\partial \mathbf{x}}{\partial \alpha_k} + \frac{\partial \mathbf{f}}{\partial \alpha_k}$$

The costate system for each parameter of interest can be integrated along with the original system, yielding the desired sensitivity functions.

Glossary

I_{Na}	Na^+ current
$I_{Ca,L}$	L-type Ca^{2+} current
I_t	Transient outward K^+ current
I_{sus}	Sustained outward K^+ current
$I_{K,s}$	Slow delayed rectifier K^+ current
$I_{K,r}$	Rapid delayed rectifier K^+ current
I_{K1}	Inwardly rectifying K^+ current
$I_{B,Na}$	Background Na^+ current
$I_{B,Ca}$	Background Ca^{2+} current
I_{NaK}	Na^+-K^+ pump current
I_{CaP}	Sarcolemmal Ca^{2+} pump current
I_{NaCa}	Na^+-Ca^{2+} exchange current
$\Phi_{Na,en}$	Electroneutral Na^+ influx
I_{di}	Ca^{2+} diffusion current from the diffusion-restricted subsarcolemmal space to the cytosol
I_{up}	Sarcoplasmic reticulum Ca^{2+} uptake current
I_{tr}	Sarcoplasmic reticulum Ca^{2+} translocation current (from uptake to release compartment)
I_{rel}	Sarcoplasmic reticulum Ca^{2+} release current
$[Na^+]_b$	Na^+ concentration in bulk (bathing) medium
$[K^+]_b$	K^+ concentration in bulk (bathing) medium
$[Ca^{2+}]_b$	Ca^{2+} concentration in bulk (bathing) medium
$[Na^+]_c$	Na^+ concentration in the extracellular cleft space
$[K^+]_c$	K^+ concentration in the extracellular cleft space
$[Ca^{2+}]_c$	Ca^{2+} concentration in the extracellular cleft space
$[Na^+]_i$	Na^+ concentration in the intracellular medium
$[K^+]_i$	K^+ concentration in the intracellular medium
$[Ca^{2+}]_i$	Ca^{2+} concentration in the intracellular medium
$[Mg^{2+}]_i$	Mg^{2+} concentration in the intracellular medium
$[Ca^{2+}]_d$	Ca^{2+} concentration in the restricted subsarcolemmal space
$[Ca^{2+}]_{up}$	Ca^{2+} concentration in the sarcoplasmic reticulum uptake compartment
$[Ca^{2+}]_{rel}$	Ca^{2+} concentration in the sarcoplasmic reticulum release compartment
E_{Na}	Equilibrium (Nernst) potential for Na^+
E_K	Equilibrium (Nernst) potential for K^+
E_{Ca}	Equilibrium (Nernst) potential for Ca^{2+}
$E_{Ca,app}$	Apparent reversal potential for $I_{Ca,L}$ (differs from E_{Ca})
P_{Na}	Permeability for I_{Na}
$\bar{g}_{Ca,L}$	Maximum conductance for $I_{Ca,L}$
$\bar{g}_t$	Maximum conductance for I_t
$\bar{g}_{sus}$	Maximum conductance for I_{sus}
$\bar{g}_{K,s}$	Maximum conductance for $I_{K,s}$
$\bar{g}_{K,r}$	Maximum conductance for $I_{K,r}$
$\bar{g}_{K1}$	Maximum conductance for I_{K1}
$\bar{g}_{B,Na}$	Maximum conductance for $I_{B,Na}$
$\bar{g}_{B,Ca}$	Maximum conductance for $I_{B,Ca}$
m	Activation gating variable for I_{Na}
h_1, h_2	Fast and slow inactivation gating variables for I_{Na}
d_L	Activation gating variable for $I_{Ca,L}$
f_{L_1}, f_{L_2}	Fast and slow inactivation gating variables for $I_{Ca,L}$
f_{Ca}	$[Ca^{2+}]_d$-dependent ratio of fast (f_{L_1}) to slow (f_{L_2}) inactivation of $I_{Ca,L}$
k_{Ca}	Half-maximum Ca^{2+} binding concentration for f_{Ca}
r	Activation gating variable for I_t
s	Inactivation gating variable for I_t
s_1, s_2	Rapidly and slowly recovering inactivation gating variables for I_t
r_{sus}	Activation gating variable for I_{sus}
s_{sus}	Inactivation gating variable for I_{sus}
n	Activation gating variable for $I_{K,s}$
p_a	Activation gating variable for $I_{K,r}$
p_i	Inactivation gating variable (instantaneous) for $I_{K,r}$
$\bar{m}$, $\bar{h}_1$, . . .	Steady-state value of m, h_1, etc
F_1	Relative amount of "inactive precursor" in the I_{rel} formulation
F_2	Relative amount of "activator" in the I_{rel} formulation
τ_m	Activation time constant for I_{Na}
τ_{h_1}, τ_{h_2}	Fast and slow inactivation time constants for I_{Na}
τ_{d_L}	Activation time constant for $I_{Ca,L}$
$\tau_{f_{L_1}}$, $\tau_{f_{L_2}}$	Fast and slow inactivation time constants for $I_{Ca,L}$
τ_r	Activation time constant for I_t
τ_s	Inactivation time constant for I_t
τ_{s_1}, τ_{s_2}	Rapidly and slowly recovering inactivation time constants for I_t
$\tau_{r_{sus}}$	Activation time constant for I_{sus}
$\tau_{s_{sus}}$	Inactivation time constant for I_{sus}
τ_n	Activation time constant for $I_{K,s}$
τ_{p_a}	Activation time constant for $I_{K,r}$
O	Buffer occupancy
O_C	Fractional occupancy of the calmodulin buffer by Ca^{2+}
O_{TC}	Fractional occupancy of the troponin-Ca^{2+} buffer by Ca^{2+}
O_{TMgC}	Fractional occupancy of the troponin-Mg^{2+} buffer by Ca^{2+}
O_{TMgMg}	Fractional occupancy of the troponin-Mg^{2+} buffer by Mg^{2+}
O_{Calse}	Fractional occupancy of the calsequestrin buffer (in the sarcoplasmic reticulum release compartment) by Ca^{2+}
R	Universal gas constant
T	Absolute temperature
F	Faraday's constant
C_m	Membrane capacitance
V	Membrane voltage
Vol_c	Volume of the extracellular cleft space
Vol_i	Total cytosolic volume
Vol_d	Volume of the diffusion-restricted subsarcolemmal space
Vol_{up}	Volume of the sarcoplasmic reticulum uptake compartment
Vol_{rel}	Volume of the sarcoplasmic reticulum release compartment

τ_{Na}, τ_K, τ_{Ca}	Time constant of diffusion of Na^+, K^+, and Ca^{2+} from the bulk medium to the extracellular cleft space
τ_{di}	Time constant of diffusion from the restricted subsarcolemmal space to the cytosol
$\bar{I}_{NaK}$	Maximum Na^+-K^+ pump current
$k_{NaK,K}$	Half-maximum K^+ binding concentration for I_{NaK}
$k_{NaK,Na}$	Half-maximum Na^+ binding concentration for I_{NaK}
$\bar{I}_{CaP}$	Maximum Ca^{2+} pump current
k_{CaP}	Half-maximum Ca^{2+} binding concentration for I_{CaP}
k_{NaCa}	Scaling factor for I_{NaCa}
γ	Position of energy barrier controlling voltage dependence of I_{NaCa}
d_{NaCa}	Denominator constant for I_{NaCa}
$\bar{I}_{up}$	Maximum sarcoplasmic reticulum uptake current
k_{cyca}	Half-maximum binding concentration for $[Ca^{2+}]_i$ to I_{up}
k_{srca}	Half-maximum binding concentration for $[Ca^{2+}]_{up}$ to I_{up}
k_{xcs}	Ratio of forward to back reactions for I_{up}
τ_{tr}	Time constant of diffusion ("translocation") of Ca^{2+} from sarcoplasmic reticulum uptake to release compartment
α_{rel}	Scaling factor for I_{rel}
$k_{rel,i}$	Half-activation $[Ca^{2+}]_i$ for I_{rel}
$k_{rel,d}$	Half-activation $[Ca^{2+}]_d$ for I_{rel}
r_{recov}	Recovery rate constant for the sarcoplasmic reticulum release channel

Acknowledgments

Mr Nygren was supported in part by a stipend from a Canadian Medical Research Council group grant. Drs Fiset and Firek are grateful for the support of Alberta Heritage Foundation for Medical Research fellowships. Dr Giles is supported as a medical scientist by the Alberta Heritage Foundation for Medical Research and receives ongoing support from the Canadian Medical Research Council and the Heart and Stroke Foundation of Canada.

References

1. Shibata EF, Drury T, Refsum H, Aldrete V, Giles W. Contributions of a transient outward current to repolarization in human atrium. *Am J Physiol*. 1989;257:H1773–H1781.
2. Firek L, Giles WR. Outward currents underlying repolarization in human atrial myocytes. *Cardiovasc Res*. 1995;39:31–38.
3. DiFrancesco D, Noble D. A model of cardiac electrical activity incorporating ionic pumps and concentration changes. *Philos Trans R Soc Lond B Biol Sci*. 1985;307:353–398.
4. Hilgemann DW, Noble D. Excitation-contraction coupling and extracellular calcium transients in rabbit atrium: reconstruction of basic cellular mechanisms. *Proc R Soc Lond B Biol Sci*. 1987;230:163–205.
5. Earm YE, Noble D. A model of the single atrial cell: relation between calcium current and calcium release. *Proc R Soc Lond B Biol Sci*. 1990;240:83–96.
6. Rasmusson RL, Clark JW, Giles WR, Robinson K, Clark RB, Shibata EF, Campbell DL. A mathematical model of electrophysiological activity in a bullfrog atrial cell. *Am J Physiol*. 1990;259:H370–H389.
7. Rasmusson RL, Clark JW, Giles WR, Shibata EF, Campbell DL. A mathematical model of a bullfrog cardiac pacemaker cell. *Am J Physiol*. 1990;259:H352–H369.
8. Luo C-H, Rudy Y. A model of the ventricular cardiac action potential: depolarization, repolarization and their interaction. *Circ Res*. 1991;68:1501–1526.
9. Luo C-H, Rudy Y. A dynamic model of the cardiac ventricular action potential, I: simulations of ionic currents and concentration changes. *Circ Res*. 1994;74:1071–1096.
10. Luo C-H, Rudy Y. A dynamic model of the cardiac ventricular action potential, II: afterdepolarizations, triggered activity, and potentiation. *Circ Res*. 1994;74:1097–1113.
11. Zeng J, Laurita KR, Rosenbaum DS, Rudy Y. Two components of the delayed rectifier K^+ current in ventricular myocytes of the guinea pig type: theoretical formulation and their role in repolarization. *Circ Res*. 1995;77:140–152.
12. Demir SS, Clark JW, Murphey CR, Giles WR. A mathematical model of a rabbit sinoatrial node cell. *Am J Physiol*. 1994;266:C832–C852.
13. Lindblad DS, Murphey CR, Clark JW, Giles WR. A model of the action potential and underlying membrane currents in a rabbit atrial cell. *Am J Physiol*. 1996;271:H1666–H1691.
14. Ilnicki T. *Electrophysiological and Mechanical Measurements in Human and Rabbit Atria*. Calgary, Canada: University of Calgary; 1987. Thesis.
15. Sakakibara Y, Wasserstrom JA, Furukawa T, Jia H, Arentzen CE, Hartz RS, Singer DH. Characterization of the sodium current in single human atrial myocytes. *Circ Res*. 1992;71:535–546.
16. Sakakibara Y, Furukawa T, Singer, Donald H, Jia H, Backer CL, Arentzen CE, Wasserstrom JA. Sodium current in isolated human ventricular myocytes. *Am J Physiol*. 1993;265:H1301–H1309.
17. Wendt DJ, Starmer F, Grant AO. Na channel kinetics remain stable during perforated-patch recordings. *Am J Physiol*. 1992;263:C1234–C1240.
18. Cohen IS, Strichartz GR. On the voltage-dependent action of tetrodotoxin. *Biophys J*. 1977;17:275–279.
19. Benitah JP, Bailly P, D'Agrosa MC, Da Ponte JP, Delgado C. Slow inward current in single cells isolated from adult human ventricles. *Pflugers Arch*. 1992;421:176–187.
20. Escande D, Coulombe A, Faivre J, Coraboeuf E. Characteristics of the time-dependent slow inward current in adult human atrial single myocytes. *J Mol Cell Cardiol*. 1986;18:547–551.
21. Le Grand B, Hatem S, Deroubaix E, Couétil J-P, Coraboeuf E. Calcium current depression in isolated human atrial myocytes after cessation of chronic treatment with calcium antagonists. *Circ Res*. 1991;69:292–300.
22. Le Grand B, Hatem S, Deroubaix E, Couétil J-P, Coraboeuf E. Depressed transient outward and calcium currents in dilated human atria. *Cardiovasc Res*. 1994;28:548–556.
23. Mewes T, Ravens U. L-type calcium currents of human myocytes from ventricle of non-failing and failing hearts and from atrium. *J Mol Cell Cardiol*. 1994;26:1307–1320.
24. Ouadid H, Seguin J, Richard S, Chaptal PA, Nargeot J. Properties and modulation of Ca channels in adult human atrial cells. *J Mol Cell Cardiol*. 1991;23:41–54.
25. Li GR, Nattel S. Properties of human atrial I_{Ca} at physiological temperatures and relevance to action potential. *Am J Physiol*. 1997;272:H227–H235.
26. Ouadid H, Albat B, Nargeot J. Calcium currents in diseased human cardiac cells. *J Cardiovasc Pharmacol*. 1995;25:282–291.
27. Sun XH, Protasi F, Takahashi M, Takeshima H, Ferguson DG, Franzini-Armstrong C. Molecular architecture of membranes involved in excitation-contraction coupling of cardiac muscle. *J Cell Biol*. 1995;129:659–671.
28. Imredy JP, Yue DT. Mechanism of Ca^{2+}-sensitive inactivation of L-type Ca^{2+} channels. *Neuron*. 1994;12:1301–1318.
29. You Y, Pelzer DJ, Pelzer S. Trypsin and forskolin decrease the sensitivity of L-type calcium current to inhibition by cytoplasmic free calcium in guinea pig heart muscle cells. *Biophys J*. 1995;69:1838–1846.
30. Giles WR, Clark RB, Braun AP. Ca^{2+}-independent transient outward current in mammalian heart. In: Morad M, Ebashi S, Trautwein W, Kurachi Y, eds. *Molecular Physiology and Pharmacology of Cardiac Ion Channels and Transporters*. Amsterdam, the Netherlands: Kluwer Publishing Ltd; 1996:141–168.
31. Escande D, Coulombe A, Faivre JF, Deroubaix E, Coraboeuf E. Two types of transient outward currents in adult human atrial cells. *Am J Physiol*. 1987;252:H142–H148.
32. Gross GJ, Burke RP, Castle NA. Characterization of transient outward current in young human atrial myocytes. *Cardiovasc Res*. 1995;29:112–117.
33. Wettwer E, Amos G, Gath J, Zerkowski HR, Reidemeister JC, Ravens U. Transient outward current in human and rat ventricular myocytes. *Cardiovasc Res*. 1993;27:1662–1669.

34. Fedida D, Wible B, Wang Z, Fermini B, Faust F, Nattel S, Brown AM. Identity of a novel delayed rectifier current from human heart with a cloned K^+ channel current. *Circ Res*. 1993;73:210–216.
35. Wang Z, Fermini B, Nattel S. Sustained depolarization-induced outward current in human atrial myocytes: evidence for a novel delayed rectifier K^+ current similar to Kv1.5 cloned channel currents. *Circ Res*. 1993;73: 1061–1076.
36. Näbauer M, Beuckelmann DJ, Erdmann E. Characteristics of transient outward current in human ventricular myocytes from patients with terminal heart failure. *Circ Res*. 1993;73:386–394.
37. Agus ZS, Dukes ID, Morad M. Divalent cations modulate the transient outward current in rat ventricular myocytes. *Am J Physiol*. 1991;261: C310–C318.
38. Fermini B, Wang Z, Duan D, Nattel S. Differences in rate dependence of transient outward current in rabbit and human atrium. *Am J Physiol*. 1992;263:H1747–H1754.
39. Koidl B, Flaschberger P, Schaffer P, Pelzmann B, Bernhart E, Mächler H, Rigler B. Effects of the class III antiarrhythmic drug ambasilide on outward currents in human atrial myocytes. *Naunyn Schmiedebergs Arch Pharmacol*. 1996;353:226–232.
40. Amos GJ, Wettwer E, Metzger F, Li Q, Himmel HM, Ravens U. Differences between outward currents of human atrial and subepicardial ventricular myocytes. *J Physiol (Lond)*. 1996;491:31–50.
41. Muraki K, Imaizumi Y, Watanabe M, Habuchi Y, Giles WR. Delayed rectifier K^+ current in rabbit atrial myocytes. *Am J Physiol*. 1995;269: H524–H532.
42. Wang Z, Fermini B, Nattel S. Delayed rectifier outward current and repolarization in human atrial myocytes. *Circ Res*. 1993;73:276–285.
43. Liu S, Rasmusson RL, Campbell DL, Wang S, Strauss HC. Activation and inactivation kinetics of an E-4031-sensitive current from single ferret atrial myocytes. *Biophys J*. 1996;70:2704–2715.
44. Wang Z, Fermini B, Nattel S. Rapid and slow components of delayed rectifier current in human atrial myocytes. *Cardiovasc Res*. 1994;28: 1540–1546.
45. Sanguinetti MC, Jiang C, Curran ME, Keating MT. A mechanistic link between an inherited and an acquired cardiac arrhythmia: HERG encodes the I_{Kr} potassium channel. *Cell*. 1995;81:299–307.
46. Lide DR, ed. *CRC Handbook of Chemistry and Physics*. Cleveland, Ohio: CRC Press; 1992.
47. Kunze DL. Rate-dependent changes in extracellular potassium in the rabbit atrium. *Circ Res*. 1977;41:122–127.
48. Cohen I, Kline R. K^+ fluctuations in the extracellular spaces of cardiac muscle: evidence from the voltage-clamp and extracellular K^+-selective microelectrodes. *Circ Res*. 1982;50:1–16.
49. Parker I, Zang WJ, Wier WG. Ca^{2+} sparks involving multiple Ca^{2+} release sites along Z-lines in rat heart cells. *J Physiol (Lond)*. 1996;497:31–38.
50. Stern MD. Theory of excitation-contraction coupling in cardiac muscle. *Biophys J*. 1992;63:497–517.
51. Isenberg G, Han S. Gradation of Ca^{2+}-induced Ca^{2+} release by voltage-clamp pulse duration in potentiated guinea-pig ventricular myocytes. *J Physiol (Lond)*. 1994;480:423–438.
52. Bénardeau A, Hatem SN, Rucker-Martin C, Le Grand B, Mace L, Dervanian P, Mercadier JJ, Coraboeuf E. Contribution of Na^+/Ca^{2+} exchange to action potential of human atrial myocytes. *Am J Physiol*. 1996;271:H1151–H1161.
53. Paulsen RA, Clark JW Jr, Murphy PH, Burdine JA. Sensitivity analysis and improved identification of a systemic arterial model. *IEEE Trans Biomed Eng*. 1982;29:164–178.
54. Le Grand B, Le Heuzey JY, Perier P, Peronneau P, Lavergne T, Hatem S, Guize L. Cellular electrophysiological effects of flecainide on human atrial fibres. *Cardiovasc Res*. 1990;24:232–238.
55. Wang Z, Pelletier LC, Talajic M, Nattel S. Effects of flecainide and quinidine on human atrial action potentials: role of rate-dependence and comparison with guinea pig, rabbit, and dog tissues. *Circulation*. 1990;82: 274–283.
56. Wang Z, Fermini B, Nattel S. Effects of flecainide, quinidine, and 4-aminopyridine on transient outward and ultrarapid delayed rectifier currents in human atrial myocytes. *J Pharmacol Exp Ther*. 1995;272:184–196.
57. Kottkamp H, Haverkamp W, Borggrefe M, Breithardt G. The role of class III antiarrhythmic drugs in atrial fibrillation. In: Olsson SB, Allessie MA, Campbell RWF, eds. *Atrial Fibrillation: Mechanisms and Therapeutic Strategies*. Armonk, NY: Futura Publishing Co Inc; 1994:287–306.
58. Li G-R, Feng J, Wang Z, Fermini B, Nattel S. Adrenergic modulation of ultrarapid delayed rectifier K^+ current in human atrial myocytes. *Circ Res*. 1995;78:903–915.
59. Van Wagoner DR, Pond AL, McCarthy PM, Trimmer JS, Nerbonne JM. Outward K^+ current densities and Kv1.5 expression are reduced in chronic human atrial fibrillation. *Circ Res*. 1997;80:772–781.
60. Yue L, Feng J, Li GR, Nattel S. Transient outward and delayed rectifier currents in canine atrium: properties and role of isolation methods. *Am J Physiol*. 1996;270:H2157–H2168.
61. Clark RB, Sanchez-Chapula J, Salinas-Stefanon E, Duff HJ, Giles WR. Quinidine-induced open channel block of K^+ current in rat ventricle. *Br J Pharmacol*. 1995;115:335–343.
62. Hatem SN, Bénardeau A, Rücker-Martin C, Marty I, de Chamisso P, Villaz M, Mercadier J-J. Different compartments of sarcoplasmic reticulum participate in the excitation-contraction coupling process in human atrial myocytes. *Circ Res*. 1997;80:345–353.

Mathematical Model of an Adult Human Atrial Cell: The Role of K+ Currents in Repolarization

A. Nygren, C. Fiset, L. Firek, J. W. Clark, D. S. Lindblad, R. B. Clark and W. R. Giles

Circ Res. 1998;82:63-81
doi: 10.1161/01.RES.82.1.63
Circulation Research is published by the American Heart Association, 7272 Greenville Avenue, Dallas, TX 75231

Print ISSN: 0009-7330. Online ISSN: 1524-4571